Transport Properties of Fluid Oxygen

A. Laesecke[a]

National Institute of Standards and Technology, Center for Chemical Technology, Thermophysics Division, Boulder, CO 80303-3328

R. Krauss and K. Stephan

Institut für Technische Thermodynamik und Thermische Verfahrenstechnik, Universität Stuttgart, P. O. Box 80 11 40, D 7000 Stuttgart 80, Federal Republic of Germany

and

W. Wagner

Institut für Thermo- und Fluiddynamik, Ruhr-Universität Bochum, P. O. Box 10 21 48, D 4300 Bochum 1, Federal Republic of Germany

Received December 15, 1989; revised manuscript received March 16, 1990

Supplementing the recently completed IUPAC tables for the thermodynamic properties of oxygen, this paper presents a data evaluation of the transport properties, viscosity, and thermal conductivity. From a comprehensive literature survey the available data have been compiled, and their quality was assessed. Selected measurements were correlated to generate skeleton tables of the most reliable data along the vapor-liquid coexistence curve and for the fluid region at pressures from 0.1 to 100 MPa and at temperatures from 70 to 1400 K.

The set of correlations which was developed includes residual concept formulations as well as transport equations of state. These allow the direct calculation of viscosities and thermal conductivities from pressure and temperature as input variables. The simplified crossover model was employed to represent the enhancement of the thermal conductivity in the critical region.

Keywords: correlation; critical enhancement; data evaluation; fluid region; oxygen; recommended values; thermal conductivity; transport equation of state; viscosity.

Contents

List of Tables

[a]Author to whom correspondence may be addressed.

List of Figures

1. Introduction

Oxygen is used in many technological processes ranging from low temperature conditions in gas liquefaction to applications at high temperatures and pressures in rocket propulsion systems. The efficient design of all these processes requires an accurate knowledge of the thermophysical properties of oxygen over a particularly wide range of fluid states.

An idea of the required accuracy may be deduced by considering that the external tank of the space shuttle contains over $5 \cdot 10^5$ L of liquid oxygen which are combusted with roughly double the amount of liquid hydro-

gen during the ascent of a mission into orbit. The mechanical and thermo- and fluid-dynamic design of tanks, tubing, and the shuttle's main engines is influenced by the thermophysical property information which is used. In particular, the viscosity and thermal conductivity of oxygen are needed to calculate various flow fields and temperature distributions.[1] Renewed demand for the thermophysical properties of oxygen is arising from the challenge of developing hypersonic aircraft; these next generation aerospace projects include the European space shuttle HERMES, the National Aerospace Plane in the U.S., and the Sänger project in the Federal Republic of Germany.

The thermal and caloric properties of oxygen have been evaluated in a IUPAC project which is published as Vol. 9 of the *International Thermodynamic Tables of the Fluid State*.[2] To complement the knowledge on the thermophysical behavior of oxygen in a consistent way, we have evaluated its transport properties viscosity and thermal conductivity on the basis of the IUPAC formulations for the thermodynamic properties. This report is organized as follows: First, the key values of the thermodynamic properties of oxygen are briefly addressed. The second part discusses the evaluation of the viscosity, separately for the limit of zero density and for the remainder of the fluid region. A modified residual function is presented which is more efficient than customary formulations. The evaluation of the thermal conductivity is described subsequently. It includes an analysis of the enhancement of the thermal conductivity in the critical region and its representation by the simplified crossover model. The final chapters outline recent developments of the concept of transport equations of state. Equations have been developed by means of a new optimization method. The results of the evaluation are summarized in suggestions for further measurements to improve the tables.

2. Thermodynamic Key Data

Although transport properties are often called "nonequilibrium" properties, they are manifestations of the same dynamic molecular phenomena which determine macroscopic equilibrium properties of the substance.[3] Their relation to the thermal and caloric properties becomes obvious when the fundamental lines in the pressure-temperature plane are considered. Macroscopic features which apply to all properties of a substance in the same way are the loci of the phase equilibria. Hence, in an evaluation of transport properties values for the triple point, the critical point, and the vapor pressure curve should be consistent to those which are used in reference to thermal and caloric properties.

For molecular oxygen, these key data have been carefully measured and evaluated. We adopt the values of the IUPAC tables. The coordinates of the triple point are

$$p_t = (0.000\ 146\ 33 \pm 0.000\ 000\ 1)\ \text{MPa},$$
$$T_t = 54.361\ \text{K}.$$

The value for T_t is a primary reference point of the International Practical Temperature Scale of 1968 (IPTS-68)[4] as is the normal boiling point at 90.188 K[b]. For a better appraisal of the available transport property data it is useful to know the liquid and gas density at the triple point

$$\rho_{t,L} = 40.816\ \text{mol/L},$$
$$\rho_{t,V} = 0.003\ 237\ \text{mol/L}.$$

The critical point coordinates of oxygen are:

$$p_c = (5.043 \pm 0.002)\ \text{MPa},$$
$$T_c = (154.581 \pm 0.01)\ \text{K},$$
$$\rho_c = (13.63 \pm 0.02)\ \text{mol/L}.$$

For completeness we note that the molar mass of molecular oxygen is

$$M = 31.9988 \cdot 10^{-3}\ \text{kg/mol}.$$

In addition to these basic constants the IUPAC formulation of the reduced Helmholtz energy of oxygen was used to evaluate densities. Only for some comparisons was another equation of state employed. The second temperature derivative of the reduced Helmholtz energy of the ideal gas $A^{id}/(RT)$, Eq. (1.13) in the IUPAC monograph, is needed for the calculation of the thermal conductivity of oxygen.

3. Evaluation of the Viscosity

The viscosity of oxygen is discussed in a large number of publications. However, only 16 sets of original experimental data were selected for this evaluation. Others had to be neglected because of insufficient data or because the data are reported unsuitably for a further evaluation. The most comprehensive data sets have been obtained in laboratories which have specialized in measurements of thermophysical properties over a longer period of time. The viscosity of oxygen has been investigated repeatedly in J. Kestin's laboratory at Brown University and in the laboratory at Leuven. Other measurements have been conducted in Japanese, Russian, and British laboratories and with the low-temperature viscometer of NIST, Boulder.

The capillary viscometer is the most frequently used experimental arrangement. Here, the nonequilibrium

[b]For the International Temperature Scale of 1990 (ITS-90), however, only the triple point of oxygen was retained as a primary reference point with the slightly differing temperature $T_t = 54.3584$ K. For details see H. Preston-Thomas, Metrologia, 27, 3 (1990).

condition necessary to obtain the viscosity is induced by moving the fluid under investigation. In the oscillating disk and torsionally vibrating quartz method, nonequilibrium is generated by moving the boundaries in contact with the fluid. These methods allow for a higher precision but require also a more complicated setup to record the signal from which the viscosity can be calculated. Two data sets have been obtained with a rolling ball instrument which involves the highest uncertainties among all the commonly used methods to measure viscosity. It is, however, a suitable method for measurements at high pressures.

None of the data sources indicate an enhancement of the viscosity when the critical point of oxygen is approached. To establish the recommended data set we applied consequently the residual concept in its simple form. The temperature and density dependence of the viscosity is considered a sum of two contributions: the viscosity in the dilute gas state, $\eta_0(T)$, which is only a function of temperature, and the excess or residual viscosity, $\Delta\eta(\rho)$, which is only density-dependent:

$$\eta(\rho,T) = \eta_0(T) + \Delta\eta(\rho). \tag{1}$$

The sole density dependence of $\Delta\eta(\rho)$ cannot be taken for granted for all substances universally. It has to be examined in every case by plotting this quantity as a function of density before a correlation is attempted.

3.1. Viscosity in the Zero-Density Limit

Since oxygen is a small diatomic molecule the temperature dependence of its viscosity in the dilute gas state or zero-density limit can be well represented by expressions derived from kinetic theory. The viscosity is given by

$$\eta_0(T)=\frac{5}{16}\cdot\sqrt{\frac{MkT}{\pi N_A}}\cdot\frac{1}{\sigma^2\Omega_\eta(T^*)} \tag{2}$$

with the absolute temperature T, the molar mass M, Boltzmann's constant k, and Avogadro's number N_A. Adjustable parameters are the length- and energy-scaling parameters σ and ϵ/k as well as the b_i's in the formulation of the collision integral Ω_η as a function of the dimensionless temperature $T^*=kT/\epsilon$, where

$$\ln\,\Omega_\eta(T^*) = \sum_{i=0}^{4} b_i\,(\ln T^*)^i. \tag{3}$$

The correlation is based on the more recent data of Clifford *et al.*,[5] Matthews *et al.*,[6] Lavushchev and Lyusternik[7] as well as the low-density data of Kestin and Leidenfrost[8] and Golubev.[9] The parameters of the above functions were obtained from a weighted nonlinear least-squares fit as follows:

$\sigma = 0.343\ 188\ 67\cdot10^{-9}$ m, $\epsilon/k = 116.2$ K,

and

$b_0 = 0.466\ 49$, $b_1 = -0.570\ 15$, $b_2 = 0.191\ 64$, $b_3 = -0.037\ 08$, $b_4 = 0.002\ 41$.

The resulting viscosity of oxygen in the zero density limit is illustrated in Fig. 1 up to 1400 K. Graphical comparisons with experimental data and previous correlations are presented in Figs. 2 to 4. Additional numerical information is provided in Table 1. Figure 2 illustrates percentage deviations of five literature data sets and two previous correlations from the present correlation up to 500 K. Although not being considered in the fit of Eq. (2), the low-density data by Kiyama and Makita[10] and Makita[11] agree with the correlation to within ±1%. The low-density data by Haynes[12] also agree well with the correlation but appear systematically lower with a maximum deviation of −1.9% at 170 K. The evaluation by Hanley, McCarty, and Sengers[13] reports viscosities which agree excellently with the present correlation above 150 K while the discrepancies amount up to 3.5% below that temperature. A similar trend is exhibited by the correlation of Younglove[14] which appears to be a refit of the work of Hanley and Ely[15] displayed in Fig. 4. The deviations reach up to 5.5% at 70 K with an almost constant offset of −0.5% from 150 K to 400 K.

Experimental data sets which cover an extended temperature range up to 2000 K are compared in Fig. 3. The mutual agreement is well within ±1% with the exception of one point by Matthews *et al.*[6] at 120 K. The data by Hellemans, Kestin, and Ro[16] exceed this threshold at 423.15 K and above, appearing systematically too high with a trend not confirmed by other measurements. Accordingly, this data set was not included in the database for the correlation. Also omitted were the measurements of Raw and Ellis[17] which yielded lower viscosities than all other investigations. Two data points with deviations below −2% fall outside the range of Fig. 3. Although somewhat lower over most of the temperature range shown, the data of Lavushchev and Lyusternik[7] join very well to the data by Matthews *et al.*[6] above 1500 K.

Results from previous evaluations are compared with the present correlation in Fig. 4 covering a temperature range up to 2800 K. Since the experimental data are limited to 2000 K this comparison indicates the suitability of the correlation for extrapolation. Three different trends are revealed by the diagram. Most noteworthy are the discrepancies which exist between the present correlation and the low-density data of the tables by Vargaftik[18] which are identical to those published later by Stephan and Lucas.[19] The deviations decrease from 4% at 100 K to −6.3% at 1300 K (not shown in Fig. 4). Congruent deviations are obtained from the low-density viscosities tabulated above 240 K in the data book of the Japanese Society of Mechanical Engineers,[20] apparently also adopted from Vargaftik. This trend, however, is in contradiction not only to the experimental data above 400 K but also to the remaining evaluations. Those by Maitland and Smith,[21] Cole and Wakeham,[22] and Bousheri *et al.*[23] form a second group differing from the results of Hanley and Ely[15] because of different data assessments. Al-

TABLE 1. Comparison of the evaluated viscosity with other data sources[a]

Authors	Year[Ref]	T, K	p, MPa	Method	$\Delta_{av}\pm s$	Δ_{max}	Δ_{min}	Data
Rudenko, Shubnikov	1934[24]	54–90	0.1	CP	−0.5±3.9	7.4	−8.6	15[b]
Makita	1955[11]	298–473	0.1–10	RB	5.0±5.0	17.0	−1.1	30
Kiyama, Makita	1956[10]	298–373	0.1–80	RB	5.5±3.8	10.5	−0.7	24
Raw, Ellis	1958[17]	960–1290	Dil. gas	CP	−1.9±1.0	−0.87	−3.6	8
Kestin, Leidenfrost	1959[8]	293–298	0.01–5.2	OD	−0.13±0.4	1.1	−0.31	15
Saji, Okuda	1964[27]	80–87	0.1	CP	1.5±0.4	2.0	0.98	5
Van Itterbeek, Hellemans, Zink, van Cauteren	1966[30]	70–90	0.01–9.7	OD	8.8±3.3	15.3	2.8	31[c]
De Bock, Grevendonk, Awouters	1967[31]	77	0.2–13.4	TVQ	−3.0±2.4	0.45	−7.0	17
Grevendonk, Herremann, de Pesseroey, de Bock	1968[28]	77 −150	0.7–19	TVQ	6.7±3.8	20.0	0.25	92
Golubev	1970[9]	288–373	0.1–70	CP	−0.12±1.0	2.96	−1.2	36
Hellemans, Zink, van Paemel	1970[29]	96–152	0.2–9.8	OD	−6.2±11.3	9.5	−37.1	44[d]
Hellemans, Kestin, Ro	1973[16]	298–770	Dil. gas	OD	0.8±0.5	1.37	−0.1	12
Clifford, Gray, Scott	1975[5]	321–1300	Dil. gas	CP	−0.3±0.4	0.24	−0.94	9
Matthews, Thomas, Duffy, Smith	1976[6]	120–1700	Dil. gas	CP	0.05±0.6	1.26	−0.96	15
Lavushchev, Lyusternik	1976[7]	400–1993	Dil. gas	CP	−0.24±0.29	0.35	−0.78	73
Haynes	1977[12]	90–300	0.1–34	TVQ	−0.6±2.0	5.6	−3.8	171
Previous evaluations:								
Maitland, Smith	1972[21]	80–1300	Dil. gas		1.21±2.2	9.7	−0.6	22
Hanley, Ely	1973[15]	80–2000	Dil. gas		−0.22±0.8	3.66	−0.8	40
Hanley, McCarty, Sengers	1974[13]	80–400	0.1–20		12.8±9.7	39.2	−0.3	792
Vargaftik and Stephan, Lucas	1975[18] 1979[19]	75–1300	0.1–100		0.9±2.1	10.2	−4.3	1206
Younglove	1982[14]	80–400	0.02–100		0.09±4.4	5.5	−51.7	1410
JSME	1983[20]	240–1300	0.1–100		−0.37±1.7	2.6	−17.3	472
Cole, Wakeham	1984[22]	120–2600	Dil. gas		0.4±0.65	1.2	−0.9	47
Bousheri, Bzowski, Kestin, Mason	1987[23]	150–2800	Dil. gas		0.75±0.36	1.1	−0.26	26

[a]Explanation: Authors whose data sets have been selected are printed in **bold face**. $\Delta_{av}\pm s$ is the percent average and its standard deviation compared to the correlation, Eqs. (2) and (4). Δ_{max} and Δ_{min} are the extreme deviations of this comparison. **CP** – Capillary viscometer, **RB** – Rolling ball viscometer, **OD** – Oscillating disk viscometer, **TVQ** – Torsionally vibrating quartz viscometer.

[b]Last data point at 54.4 K omitted.

[c]Second data point omitted.

[d]Five data points with deviations of more than 100% disregarded.

though completed almost simultaneously and with the same experimental data base, the correlations by Maitland and Smith[21] and Hanley and Ely[15] disagree mutually by nearly 2% above 600 K. The viscosities by Maitland and Smith above 280 K are estimates with the point at 1200 K substantially deviating from the general trend of the other values. The correlation of Cole and Wakeham supports the work of Hanley and Ely except in the temperature range 300 to 1500 K where it is based on the data by Hellemans, Kestin, and Ro (discussed above), and the data by Matthews *et al.* which were not available at the time Hanley and Ely evaluated the viscosity of dilute oxygen. The most recent evaluation by Bousheri *et al.*[23] emphasizes almost exclusively the data of Hellemans, Kestin, and Ro, and ignores the measurements of Lavushchev and Lyusternik;[7] this results in differences of 1 to 1.5% to the present correlation above 400 K. However, at temperatures below 300 K this evaluation is the only one which confirms the data assessment of this work within ±0.5%.

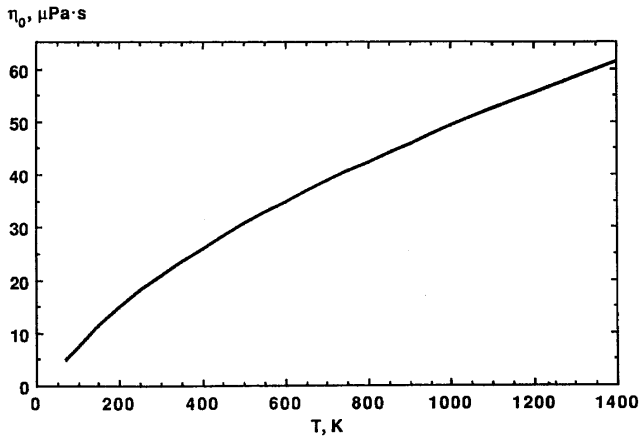

FIG. 1. The viscosity of oxygen at zero density, Eq. (2).

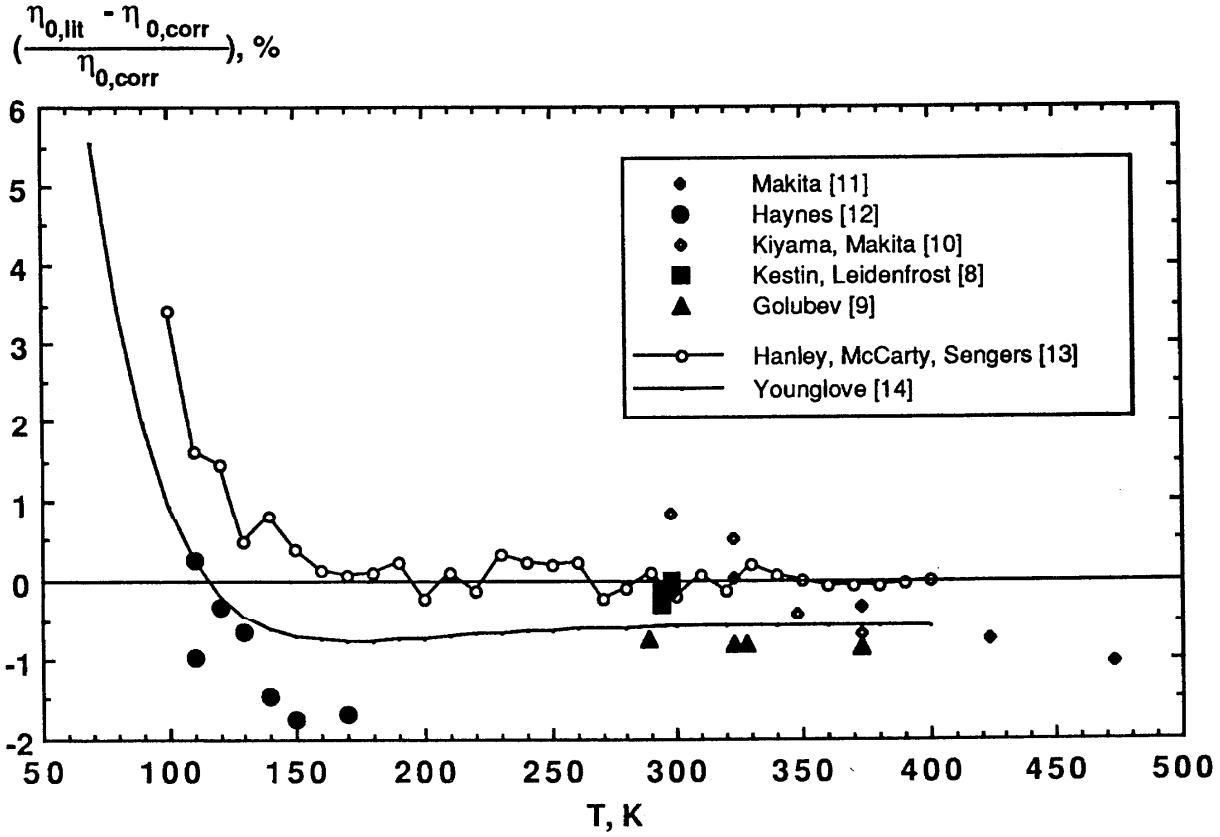

FIG. 2. Percentage deviations of literature data and previous correlations from the present correlation for the viscosity of oxygen at zero-density and temperatures up to 500 K.

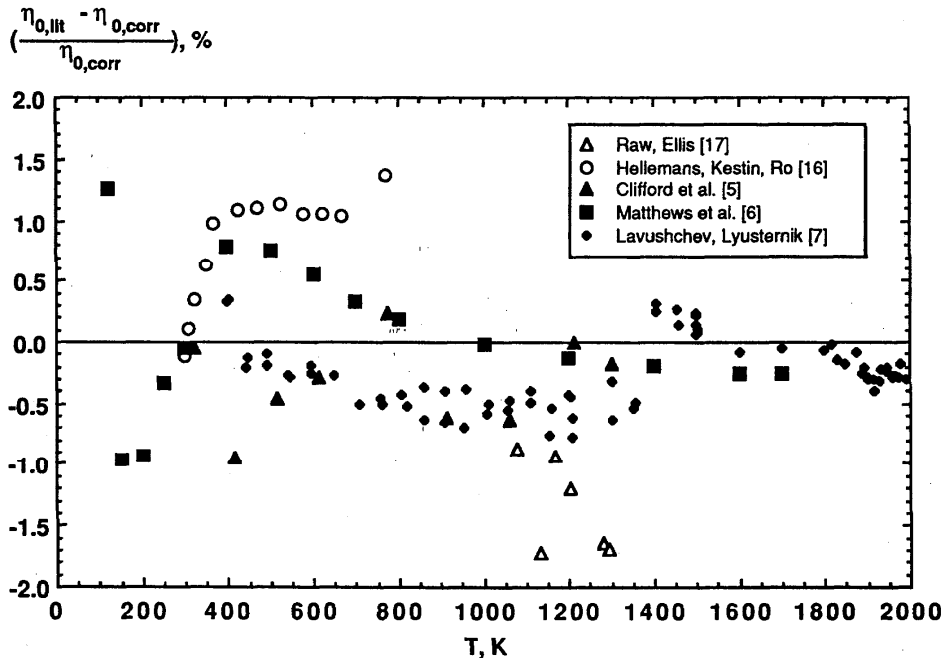

FIG. 3. Percentage deviations of literature data from the present correlation for the viscosity of oxygen at zero-density and temperatures up to 2000 K.

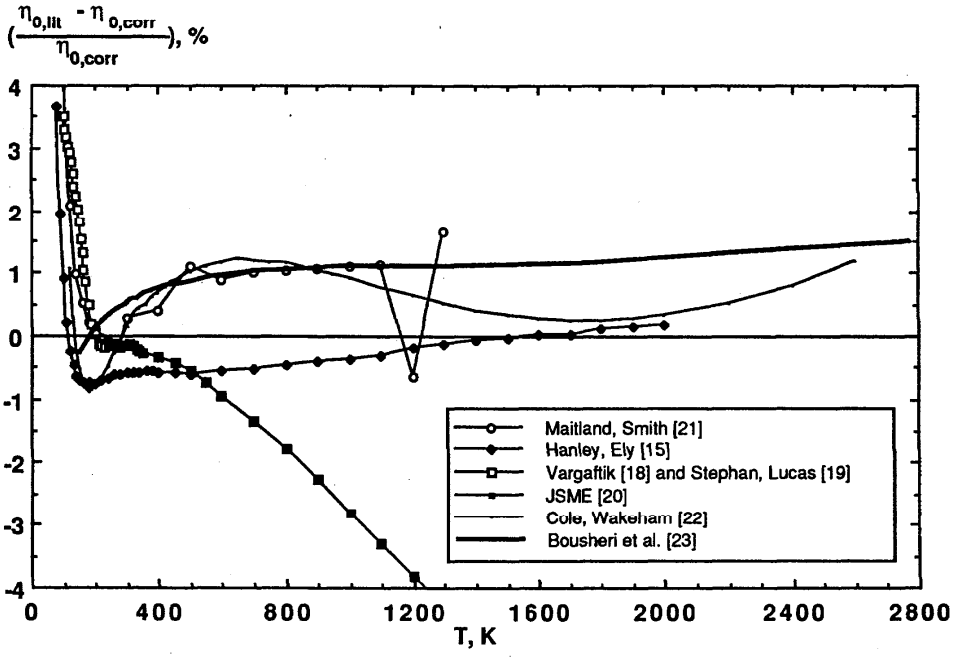

FIG. 4. Percentage deviations of previous correlations from the present correlation for the viscosity of oxygen at zero density and temperatures up to 2800 K.

3.2. The Residual Viscosity

Nine experimental data sets which provide information about the pressure dependence of the viscosity of oxygen were included in this study. Thanks to the measurements of Rudenko and Shubnikov[24] the data reach close to the triple point density. They were used for the correlation together with the data of Kestin and Leidenfrost,[8] Golubev,[9] and Haynes.[12]

The extremely steep rise of the viscosity at very high densities cannot be described satisfactorily with customary density functions. Hence, a variety of functional forms was tested for the correlation. A temperature dependence was not included since the experimental evidence is limited to the 90 K and 110 K isotherms of the measurements by Haynes. The residual viscosities as extracted from the selected data were represented best by a third-degree polynomial combined with a hyperbolic term,

$$\frac{\Delta\eta(\rho)}{H} = \frac{c_0}{\rho_R - \rho_{Rt}} + \frac{c_0}{\rho_{Rt}} + \sum_{i=1}^{3} c_i \cdot \rho_R^i, \qquad (4)$$

as a function of the reduced density $\rho_R = \rho/\rho_c$. The values of the adjustable parameters were obtained from a nonlinear fit of weighted least squares as follows

$$c_0 = -5.602\ 882\ 07, \quad c_1 = -0.397\ 230\ 772,$$
$$c_2 = 0.312\ 536\ 267, \quad c_3 = -0.0615\ 559\ 341,$$
$$\rho_{Rt} = 3.113\ 811\ 2.$$

The value of parameter ρ_{Rt} which marks the singularity of Eq. (4) corresponds to a density of $\rho = 42.441$ mol/L located in the solid region of oxygen.

The factor H is used to express the residual viscosity in dimensionless form. Unlike thermodynamic properties, critical values of the transport properties cannot practically be used as reducing constants. In light of the scaling-law hypothesis the transport properties become infinite at the critical point. The determination of a critical value from the "background" contribution implies usually a considerable uncertainty because of the scatter of the experimental data in that region. To obtain a reliable and substance-characteristic value for the viscosity, the factor

$$H = \frac{M^{1/2} p_c^{2/3}}{R^{1/6} N_A^{1/3} T_c^{1/6}} = \frac{m^{1/2} p_c^{2/3}}{(k \cdot T_c)^{1/6}} \qquad (5)$$

was chosen to calculate reduced quantities. It was derived first by Kamerlingh Onnes[25] and includes the critical pressure p_c, the critical temperature T_c, the molar mass M, or the molecular mass $m = M/N_A$, which are usually known with high accuracy. R is the universal gas constant, k is Boltzmann's constant, and N_A is Avogadro's constant. H yields a value of 18.8928 μPa·s for oxygen; this corresponds to the viscosity of a state point in the supercritical gas region at approximately 7 MPa and 240 K (cf. Table 4).

The residual viscosity of oxygen as calculated from Eq. (4) is depicted in Fig. 5 accompanied by comparisons with original data in Figs. 6 and 7. Additional numerical information is listed in Table 1. All deviations are calculated in terms of the viscosity $\eta(\rho,T)$ rather than in terms of only the residual part $\eta(\rho)$. The four data sets on which the correlation is based are included in the deviation plot, Fig. 6. The bulk of the data was obtained by Haynes[12] in the torsionally vibrating quartz viscometer at NIST, Boulder, and shows an internal consistency of about ±2% up to 32 mol/L. The Golubev[9] measurements in a capillary viscometer appear to coincide with the arithmetic average of Haynes's data, both sets being reproduced by the correlation in a slightly wavy manner. An additional temperature dependence of the viscosity of oxygen can be discriminated from the 110 K and 90 K isotherms of Haynes above 32 mol/L, but this experimental evidence appeared too limited to attempt a more complicated formulation of the residual viscosity by including temperature terms with additional adjustable parameters. It is likely that the wide ranging deviations (±8%) of the data by Rudenko and Shubnikov[24] are partially due to this characteristic, too. In addition, however, the experimental uncertainty of these measurements has to be estimated higher than claimed by the authors (1.4%) since they were carried out in Ubbelohde viscometers with manual timing, because of uncertainties of the temperature measurement which become very significant in the liquid region, and because the densities which were used to evaluate the viscosities remain unclear. Saturated liquid viscosities reported by Rudenko[26] in 1939 appeared to be erroneous and were rejected.

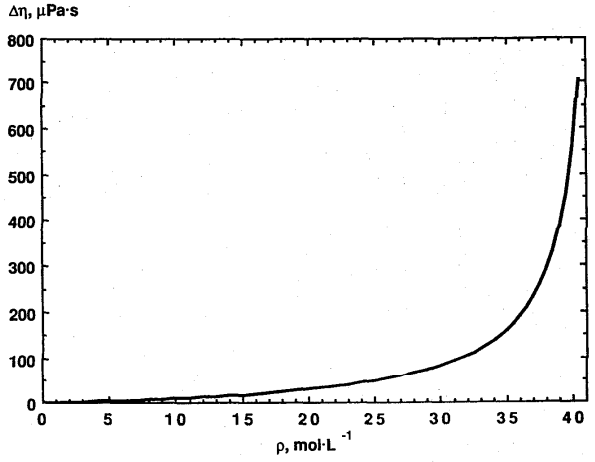

FIG. 5. The residual viscosity of oxygen, Eq. (4).

Vast and mostly systematic discrepancies are found when the correlation is compared with the remaining data sets, Fig. 7. An exception are the five data points by Saji and Okuda[27] with a maximum deviation of 2%. The

only other measurements below 20 mol/L are those of Kiyama and Makita,[10] and Makita,[11] who reported up to 17% higher viscosities. The density region above 25 mol/L was explored in four studies at Leuven with partially contradicting results. This holds in particular for the measurements of Grevendonk *et al.*[28] with deviations up to 20% and the measurements of Hellemans, Zink, and van Paemel[29] with deviations down to −37% (not shown in Fig. 7). The earlier data by van Itterbeek *et al.*[30] cover densities above 35 mol/L but are systematically too high. The 77 K isotherm measured by de Bock *et al.*[31] points towards the above mentioned temperature dependence of the viscosity at high densities but does not join well to the data of Haynes, although the same type of viscometer was used in both studies.

The results of this correlation are finally compared with the viscosity of oxygen as reported in several previous evaluations. The earliest data assessment was carried out by Hanley, McCarty, and Sengers[13] in 1974 when the experimental information was yet rather limited. In fact, the evaluation was based mainly on the data set by Grevendonk *et al.*, which is identified in this analysis as too high. The statistical measures in Table 1 confirm this for the evaluated tables of Hanley, McCarty, and Sengers. A second report was published by Hanley, McCarty, and Haynes[32] in the same year but will not be discussed here since it has been superseded by the more recent correlation of Younglove[14] which is equal to the one by Roder.[33] These viscosities are in better agreement with the present results but tend to be too low at high pressures/densities with deviations of as much as −51.7%. The tables of Vargaftik[18] as adopted by Stephan and Lucas[19] show the same trend as illustrated in Fig. 4 for the dilute gas region, that is positive deviations at low temperature versus negative deviations at elevated temperatures. Almost identical tables were published by the Japanese Society of Mechanical Engineers (JSME)[20] except that the temperature range is limited to 240 K and above. Figure 8 is a representative example of these trends showing the relative deviations of the previously evaluated data from the present correlation along the near-critical 5 MPa isobar.

Viscosity values which were calculated from the newly established correlation are presented in Table 3 for the saturation boundary and in Table 4 for the entire fluid region in a pressure range from 0.1 to 100 MPa and for temperatures from 70 to 1400 K.

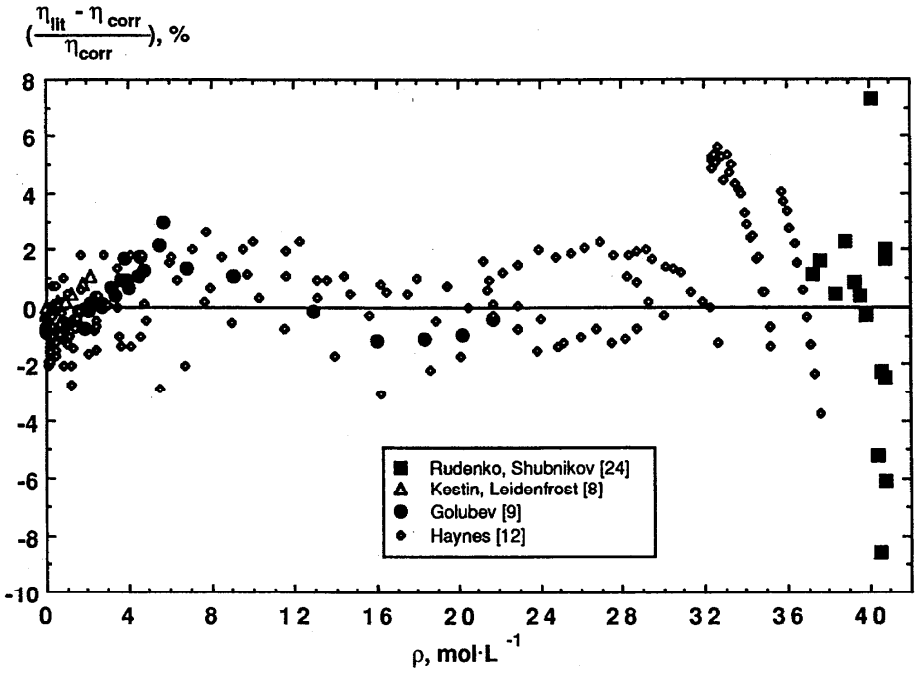

FIG. 6. Percentage deviations of the selected data sets from the correlation for the viscosity of oxygen.

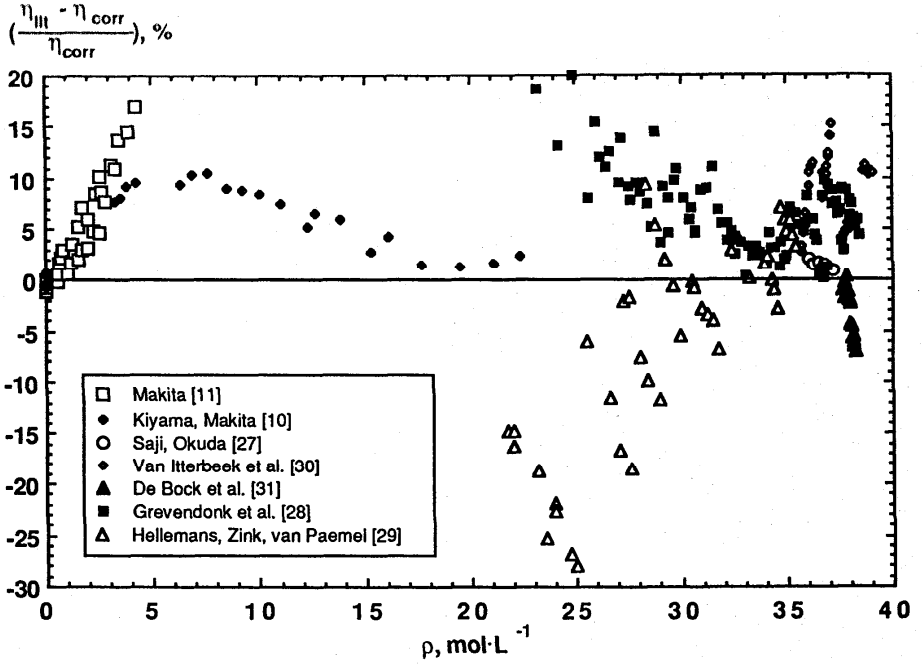

FIG. 7. Percentage deviations of data sets which were not selected from the correlation for the viscosity of oxygen.

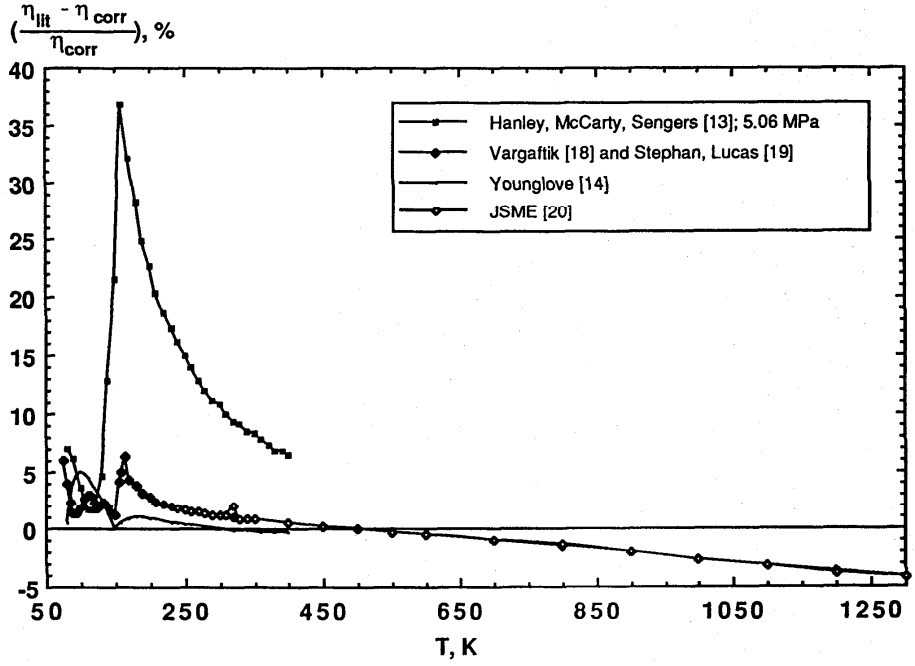

FIG. 8. Percentage deviations of previously evaluated data from the correlation for the viscosity of oxygen, along the 5 MPa isobar.

TABLE 2. Comparison of the evaluated thermal conductivity of oxygen with other data sources[a]

Authors	Year[Ref]	T, K	p, MPa	Method	$\Delta_{av}\pm s$	Δ_{max}	Δ_{min}	Data
Johnston, Grilly	1946[44]	86–376	Dil. gas	SH	0.17±2.5	5.5	−2.7	18
Borovik	1947[39]	156	0.1–9.8	PP	−2.0±6.9	5.6	−12	5
Franck	1951[49]	93–787	Dil. gas	SH	−1.2±2.6	2.9	−2.3	13
Keyes	1955[37]	97–273	0.1–1.1	CC	−0.28±1.3	1.3	−2.3	7
Ziebland, Burton	1956[38]	79–199	0.1–13.7	CC	3.3±6.5	24	−3.6	65
Tsederberg	1957[45]	73–313	0.1–9.8	SH	1.3±3.8	10.5	−6.5	78
Geier, Schäfer	1961[41]	273–1373	Dil. gas	SH	1.4±0.55	2.3	0.04	12
Pereira, Raw	1963[47]	305–453	Dil. gas	SH	2.7±0.85	4.0	1.9	5
Westenberg, de Haas	1963[50]	300–1200	Dil. gas	SH	1.14±1.1	3.1	−0.2	10
Ivanova, Tsederberg, Popov	1967[46]	73–373	0.1–49	SH	1.8±4.2	9.8	−7.5	112
Saxena, Gupta	1970[42]	350–1500	Dil. gas	SH	−0.66±1.6	2.9	−2.3	13
Jain, Saxena	1977[43]	400–1600	Dil. gas	SH	−0.27±1.6	3.0	−1.9	13
Roder	1982[35]	77–310	0.1–65	TH	0.03±1.0	2.9	−2.7	202[b]
Data sets which report a critical enhancement:								
Roder	1982[35]	144–179	2.6–13	TH	−0.25±4.0	10.7	−13.3	104[c]
Weber	1982[36]	153–174	density	LS	3.0±13.6	42.7	−46.6	70[d]
Previous evaluations:								
Vassermann, Rabinovich	1970[48]	75–180	0.1–50		−0.65±1.4	5.8	−3.1	542
Touloukian, Liley, Saxena	1970[51]	100–1500	Dil. gas		1.5±1.3	2.9	−2.7	15
Hanley, Ely	1973[15]	80–2000	Dil. gas		−1.5±3.2	6.7	−2.5	42
Hanley, McCarty, Sengers	1974[13]	80–400	0.1–20.2		6.1±5.6	37.9	−2	792
Vargaftik, Filippov, Tarzimanov, Tozkij	1978[52]	80–1400	0.1–60		1.1±3.8	11.3	−9.5	720
Younglove	1982[14]	80–400	0.02–100		−0.5±6.9	21.3	−28.	1410[e]
JSME	1983[20]	75–265	0.01–35		−0.6±7.7	65	−13.7	773

[a]Explanation: Authors whose data sets have been selected are printed in **bold face**. $\Delta_{av}\pm s$ is the percent average and its standard deviation compared to the correlation, Eqs. (8) and (9). Δ_{max} and Δ_{min} are the extreme deviations of this comparison. **CC** – Coaxial cylinder instrument, **LS** – Rayleigh light scattering technique, **PP** – Parallel plate method, **SH** – Steady-state hot-wire instrument, **TH** – Transient hot-wire instrument.

[b]Only data without critical enhancement used.

[c]Selected data with critical enhancement compared with new correlation and simplified crossover model using $q_{D,av}^{-1} = 0.4167$ nm (see Fig. 26).

[d]Six data points omitted. Comparison with new correlation and simplified crossover model using $q_{D,av}^{-1} = 0.4167$ nm (see Fig. 27).

[e]Comparison without critical enhancement.

TABLE 3. Viscosity (μPa·s) and thermal conductivity (mW/(m·K)) of oxygen along the saturation curve[a]

T, K	p_s, MPa	η_L	η_V	λ_L	λ_V
70	$0.6262 \cdot 10^{-2}$	355.0	4.776	181.3	5.981
71	$0.7490 \cdot 10^{-2}$	340.9	4.865	179.9	6.093
72	$0.8910 \cdot 10^{-2}$	327.8	4.954	178.5	6.205
73	$0.1054 \cdot 10^{-1}$	315.6	5.042	177.1	6.317
74	$0.1241 \cdot 10^{-1}$	304.2	5.131	175.7	6.429
75	$0.1455 \cdot 10^{-1}$	293.4	5.219	174.2	6.541
76	$0.1697 \cdot 10^{-1}$	283.3	5.308	172.8	6.654
77	$0.1971 \cdot 10^{-1}$	273.9	5.396	171.4	6.766
78	$0.2279 \cdot 10^{-1}$	264.9	5.484	170.0	6.879
79	$0.2625 \cdot 10^{-1}$	256.5	5.573	168.6	6.992
80	$0.3012 \cdot 10^{-1}$	248.4	5.661	167.2	7.105
81	$0.3444 \cdot 10^{-1}$	240.9	5.749	165.8	7.219
82	$0.3923 \cdot 10^{-1}$	233.7	5.838	164.3	7.333
83	$0.4453 \cdot 10^{-1}$	226.8	5.926	162.9	7.447
84	$0.5039 \cdot 10^{-1}$	220.3	6.014	161.5	7.561
85	$0.5683 \cdot 10^{-1}$	214.1	6.102	160.1	7.676
86	$0.6391 \cdot 10^{-1}$	208.2	6.190	158.7	7.792
87	$0.7165 \cdot 10^{-1}$	202.5	6.279	157.3	7.907
88	$0.8011 \cdot 10^{-1}$	197.1	6.367	155.9	8.024
89	$0.8933 \cdot 10^{-1}$	191.9	6.455	154.5	8.141
90	$0.9935 \cdot 10^{-1}$	186.9	6.544	153.1	8.258
90.188	0.1013	186.0	6.561	152.8	8.280
91	0.1102	182.1	6.633	151.7	8.376
92	0.1220	177.6	6.721	150.3	8.495
93	0.1347	173.2	6.810	148.8	8.615
94	0.1484	168.9	6.899	147.4	8.735
95	0.1631	164.8	6.988	146.0	8.856
96	0.1789	160.9	7.077	144.6	8.978
97	0.1958	157.1	7.167	143.2	9.101
98	0.2140	153.4	7.256	141.8	9.225
99	0.2333	149.9	7.346	140.4	9.351
100	0.2540	146.4	7.436	139.0	9.477
101	0.2760	143.1	7.527	137.6	9.605
102	0.2994	139.9	7.617	136.1	9.734
103	0.3243	136.8	7.708	134.7	9.864
104	0.3506	133.8	7.800	133.3	9.996
105	0.3785	130.8	7.892	131.9	10.13
106	0.4081	128.0	7.984	130.5	10.26
107	0.4393	125.2	8.077	129.0	10.40
108	0.4722	122.5	8.170	127.6	10.54
109	0.5069	119.9	8.264	126.2	10.68
110	0.5434	117.4	8.359	124.8	10.82
111	0.5818	114.9	8.454	123.3	10.97
112	0.6222	112.4	8.550	121.9	11.12
113	0.6646	110.1	8.647	120.5	11.27
114	0.7091	107.8	8.745	119.0	11.42
115	0.7556	105.5	8.844	117.6	11.58
116	0.8044	103.3	8.943	116.2	11.74
117	0.8554	101.2	9.044	114.7	11.90
118	0.9086	99.05	9.146	113.3	12.06
119	0.9643	96.98	9.250	111.8	12.23
120	1.022	94.96	9.355	110.3	12.41
121	1.083	92.98	9.461	108.9	12.58
122	1.146	91.03	9.569	107.4	12.77
123	1.212	89.12	9.679	105.9	12.95
124	1.280	87.24	9.791	104.5	13.15
125	1.351	85.40	9.905	103.0	13.34
126	1.425	83.58	10.02	101.5	13.55
127	1.501	81.79	10.14	99.99	13.76
128	1.581	80.03	10.26	98.48	13.98
129	1.663	78.29	10.39	96.97	14.20
130	1.749	76.58	10.52	95.44	14.44
131	1.838	74.88	10.65	93.91	14.68
132	1.930	73.21	10.79	92.37	14.93
133	2.025	71.55	10.93	90.81	15.19
134	2.123	69.91	11.07	89.24	15.46
135	2.225	68.28	11.23	87.66	15.75
136	2.330	66.66	11.39	86.06	16.05
137	2.439	65.05	11.55	84.44	16.36
138	2.552	63.45	11.73	82.81	16.69
139	2.668	61.85	11.91	81.15	17.04
140	2.788	60.25	12.10	79.48	17.41
141	2.912	58.65	12.31	77.77	17.80
142	3.039	57.04	12.53	76.03	18.21
143	3.171	55.43	12.76	74.26	18.65
144	3.307	53.79	13.01	72.45	19.13
145	3.448	52.14	13.29	70.59	19.65
146	3.593	50.45	13.59	68.67	20.21
147	3.742	48.72	13.93	66.69	20.83
148	3.896	46.94	14.30	64.61	21.51
149	4.055	45.09	14.73	62.43	22.28
150	4.219	43.13	15.23	60.11	23.16
151	4.388	41.02	15.84	57.58	24.20
152	4.563	38.67	16.61	54.74	25.48
153	4.743	35.90	17.68	51.35	27.20
154	4.931	32.07	19.53	46.61	30.02
154.581	**5.043**	**24.91**	**24.91**	**37.47**	**37.47**

[a]The table was generated using the IUPAC auxiliary equations for the vapor pressure, saturated liquid, and saturated vapor density. Viscosities were calculated from Eqs. (2) and (4), thermal conductivities from Eqs. (8) and (9). The table entries correspond to those of table 2 in the IUPAC monograph. Indices: s — at saturation, L — saturated liquid, V — saturated vapor.

TABLE 4. Viscosity (μPa·s) of oxygen

p, MPa	T, K 70	80	90	100	110	120	130	140	150	160	170	180
0.1	352.1	247.2	186.3	7.381	8.198	8.996	9.775	10.54	11.28	12.00	12.71	13.40
1	356.2	249.8	188.2	147.5	118.0	9.342	10.07	10.80	11.51	12.22	12.91	13.59
2	360.9	252.8	190.5	149.4	119.7	96.57	77.05	11.30	11.92	12.57	13.22	13.86
3	365.7	255.8	192.7	151.2	121.4	98.27	78.99	60.86	12.64	13.11	13.66	14.24
4	370.5	258.8	194.9	153.1	123.1	99.93	80.84	63.46	14.31	14.00	14.30	14.75
5	375.4	261.8	197.2	154.9	124.7	101.6	82.61	65.77	47.76	15.75	15.28	15.46
6	380.4	264.9	199.4	156.8	126.4	103.2	84.32	67.87	51.59	22.81	16.89	16.45
7	385.4	268.0	201.7	158.7	128.1	104.8	85.98	69.82	54.55	36.34	19.82	17.85
8	390.6	271.2	204.0	160.5	129.7	106.3	87.59	71.66	57.06	41.75	25.06	19.86
9	395.8	274.4	206.3	162.4	131.3	107.9	89.16	73.41	59.29	45.42	30.94	22.63
10	401.1	277.6	208.7	164.3	133.0	109.4	90.70	75.08	61.31	48.34	35.52	26.00
15	429.2	294.3	220.5	173.8	141.2	116.9	98.03	82.68	69.77	58.60	48.77	40.31
20	459.9	312.0	232.9	183.4	149.3	124.3	104.9	89.50	76.79	66.09	56.99	49.24
25	493.8	330.9	245.8	193.4	157.6	131.5	111.6	95.89	83.10	72.49	63.58	56.06
30	531.5	351.1	259.4	203.6	166.0	138.8	118.2	102.0	89.01	78.30	69.37	61.88
35	573.5	372.9	273.6	214.2	174.5	146.1	124.7	108.0	94.66	83.75	74.69	67.12
40	620.7	396.4	288.6	225.2	183.3	153.5	131.2	113.9	100.2	88.97	79.71	71.99
45	674.3	421.8	304.5	236.7	192.3	161.0	137.8	119.8	105.6	94.04	84.54	76.62
50	735.6	449.5	321.4	248.6	201.6	168.7	144.4	125.7	110.9	99.01	89.22	81.08
60		513.1	358.7	274.4	221.2	184.6	157.9	137.6	121.6	108.8	98.36	89.68
70		590.9	401.5	302.9	242.4	201.5	172.0	149.7	132.4	118.6	107.4	98.06
80		688.4	451.3	334.8	265.5	219.5	186.8	162.4	143.5	128.5	116.4	106.4
90		814.5	510.4	371.0	290.9	238.9	202.5	175.6	154.9	138.7	125.5	114.7
100			581.7	412.5	319.2	260.0	219.3	189.5	166.9	149.0	134.9	123.2

p, MPa	T, K 190	200	220	240	260	280	300	320	340	360	380	400
0.1	14.08	14.75	16.04	17.28	18.47	19.63	20.75	21.84	22.89	23.92	24.93	25.90
1	14.25	14.91	16.18	17.40	18.59	19.74	20.85	21.93	22.98	24.00	25.00	25.98
2	14.50	15.14	16.37	17.58	18.74	19.87	20.97	22.05	23.09	24.10	25.10	26.07
3	14.83	15.43	16.62	17.78	18.92	20.04	21.12	22.18	23.21	24.22	25.20	26.16
4	15.26	15.80	16.91	18.03	19.14	20.22	21.29	22.33	23.35	24.34	25.32	26.27
5	15.82	16.27	17.27	18.32	19.38	20.43	21.47	22.49	23.49	24.48	25.44	26.39
6	16.55	16.85	17.69	18.65	19.65	20.66	21.67	22.67	23.66	24.63	25.58	26.51
7	17.50	17.57	18.18	19.02	19.96	20.92	21.90	22.87	23.83	24.79	25.72	26.65
8	18.72	18.45	18.75	19.45	20.30	21.21	22.14	23.08	24.02	24.96	25.88	26.79
9	20.27	19.52	19.41	19.93	20.67	21.52	22.41	23.31	24.23	25.14	26.04	26.94
10	22.17	20.78	20.16	20.46	21.09	21.85	22.69	23.56	24.44	25.33	26.22	27.10
15	33.73	29.32	25.17	23.88	23.66	23.91	24.40	25.02	25.72	26.46	27.23	28.01
20	42.82	37.75	31.30	28.25	26.94	26.50	26.53	26.82	27.27	27.82	28.44	29.11
25	49.76	44.58	37.18	32.90	30.60	29.44	28.96	28.88	29.05	29.38	29.83	30.35
30	55.58	50.33	42.46	37.41	34.33	32.54	31.57	31.10	30.98	31.08	31.34	31.71
35	60.75	55.40	47.20	41.63	37.99	35.67	34.25	33.42	33.01	32.88	32.95	33.16
40	65.50	60.02	51.53	45.57	41.49	38.74	36.93	35.78	35.10	34.74	34.61	34.67
45	69.97	64.35	55.56	49.28	44.83	41.72	39.58	38.14	37.20	36.63	36.32	36.22
50	74.24	68.46	59.37	52.79	48.03	44.61	42.18	40.47	39.30	38.53	38.05	37.79
60	82.40	76.25	66.52	59.37	54.06	50.11	47.19	45.03	43.45	42.31	41.51	40.98
70	90.27	83.69	73.27	65.54	59.73	55.32	51.97	49.42	47.49	46.03	44.95	44.16
80	98.01	90.95	79.78	71.45	65.15	60.31	56.57	53.67	51.41	49.67	48.33	47.30
90	105.7	98.15	86.15	77.21	70.39	65.13	61.02	57.79	55.24	53.23	51.64	50.40
100	113.5	105.4	92.47	82.87	75.53	69.83	65.36	61.81	58.97	56.71	54.90	53.45

TABLE 4. Viscosity (μPa·s) of oxygen Continued

p, MPa	T, K 420	440	460	480	500	550	600	650	700	750	800	850
0.1	26.86	27.80	28.72	29.62	30.50	32.64	34.70	36.68	38.60	40.46	42.27	44.03
1	26.93	27.86	28.78	29.68	30.56	32.69	34.75	36.72	38.64	40.50	42.30	44.06
2	27.01	27.94	28.86	29.75	30.63	32.76	34.80	36.78	38.69	40.54	42.34	44.10
3	27.11	28.03	28.94	29.83	30.70	32.82	34.86	36.83	38.74	40.59	42.38	44.14
4	27.21	28.13	29.03	29.91	30.78	32.89	34.92	36.89	38.79	40.63	42.43	44.18
5	27.32	28.23	29.12	30.00	30.86	32.97	34.99	36.95	38.84	40.68	42.48	44.22
6	27.43	28.33	29.22	30.10	30.95	33.05	35.06	37.01	38.90	40.74	42.52	44.27
7	27.56	28.45	29.33	30.20	31.05	33.13	35.13	37.08	38.96	40.79	42.57	44.32
8	27.69	28.57	29.44	30.30	31.15	33.22	35.21	37.15	39.02	40.85	42.63	44.36
9	27.83	28.70	29.56	30.41	31.26	33.31	35.29	37.22	39.09	40.91	42.68	44.41
10	27.97	28.84	29.69	30.53	31.36	33.40	35.38	37.29	39.15	40.97	42.74	44.47
15	28.81	29.60	30.40	31.19	31.98	33.93	35.84	37.70	39.52	41.30	43.04	44.74
20	29.80	30.51	31.24	31.97	32.70	34.54	36.37	38.17	39.94	41.68	43.38	45.06
25	30.93	31.54	32.18	32.84	33.51	35.23	36.96	38.69	40.40	42.09	43.76	45.40
30	32.16	32.67	33.21	33.80	34.40	35.98	37.61	39.26	40.91	42.55	44.17	45.78
35	33.47	33.87	34.32	34.82	35.35	36.78	38.30	39.86	41.44	43.03	44.61	46.17
40	34.85	35.13	35.48	35.89	36.35	37.63	39.03	40.50	42.01	43.54	45.07	46.59
45	36.26	36.43	36.68	37.01	37.39	38.51	39.79	41.17	42.61	44.07	45.55	47.03
50	37.71	37.76	37.92	38.15	38.46	39.42	40.58	41.87	43.23	44.63	46.05	47.49
60	40.65	40.48	40.44	40.51	40.66	41.31	42.23	43.32	44.52	45.79	47.11	48.45
70	43.60	43.23	43.01	42.91	42.91	43.25	43.93	44.82	45.86	47.00	48.21	49.46
80	46.53	45.97	45.58	45.33	45.19	45.23	45.67	46.37	47.25	48.26	49.35	50.51
90	49.43	48.69	48.14	47.74	47.47	47.23	47.43	47.94	48.67	49.54	50.53	51.59
100	52.30	51.39	50.68	50.14	49.74	49.22	49.21	49.53	50.1	50.85	51.72	52.68

p, MPa	T, K 900	950	1000	1100	1200	1300	1400
0.1	45.75	47.43	49.08	52.28	55.36	58.36	61.27
1	45.78	47.46	49.10	52.30	55.39	58.38	61.29
2	45.81	47.49	49.14	52.33	55.41	58.40	61.31
3	45.85	47.53	49.17	52.36	55.44	58.43	61.34
4	45.89	47.56	49.20	52.39	55.47	58.46	61.36
5	45.93	47.60	49.24	52.42	55.50	58.48	61.38
6	45.97	47.64	49.28	52.46	55.53	58.51	61.41
7	46.02	47.68	49.31	52.49	55.56	58.54	61.44
8	46.06	47.72	49.35	52.52	55.59	58.57	61.46
9	46.11	47.77	49.39	52.56	55.62	58.60	61.49
10	46.16	47.81	49.44	52.60	55.66	58.63	61.52
15	46.41	48.05	49.66	52.79	55.83	58.78	61.66
20	46.70	48.32	49.91	53.01	56.03	58.96	61.82
25	47.02	48.61	50.18	53.25	56.24	59.15	61.99
30	47.36	48.93	50.48	53.51	56.46	59.35	62.17
35	47.73	49.27	50.79	53.78	56.70	59.56	62.37
40	48.11	49.62	51.12	54.07	56.96	59.79	62.57
45	48.52	49.99	51.46	54.37	57.22	60.03	62.78
50	48.94	50.38	51.82	54.68	57.50	60.27	63.00
60	49.82	51.20	52.58	55.34	58.08	60.79	63.47
70	50.75	52.05	53.37	56.03	58.69	61.33	63.96
80	51.71	52.95	54.20	56.75	59.33	61.91	64.47
90	52.71	53.87	55.06	57.50	59.99	62.50	65.01
100	53.72	54.81	55.94	58.27	60.67	63.11	65.56

4. Evaluation of the Thermal Conductivity

While the status of the experimental work on the viscosity of oxygen may be rated satisfactory, its thermal conductivity has been investigated to a much lesser extent. Not only is the number of studies smaller, but also the pressure and temperature ranges are not as extensive. Nevertheless, the thermal conductivity of oxygen has been the subject of measurements for more than 110 years.[34] Only fourteen sets of original data since 1946 were included in this evaluation since very early thermal conductivity experiments yielded generally too high values. The most comprehensive investigation dates from 1982 and was conducted by Roder[35] at NIST, Boulder. Because these data were obtained with a well established transient hot-wire instrument, the results of this study are considered the most reliable so far. No other thermal conductivity measurements for oxygen have been published since 1982. The work by Weber[36] explored the immediate vicinity of the critical point with the Rayleigh light-scattering technique. The reported thermal conductivity data were derived from the originally measured thermal diffusivities using density and specific heat capacity information from an equation of state.

Roder reports more data than the grand total of literature data which were available until 1982. This is indicative of the speed with which thermal conductivity can be measured in transient hot-wire instruments. The earlier data sets of Keyes[37] and Ziebland and Burton[38] were obtained in concentric cylinder instruments, while Borovik[39] used a parallel-plate arrangement for measurements along a near-critical isotherm. All other authors used hot-wire instruments under steady-state conditions.

The correlation of the thermal conductivity follows the same guidelines which were applied for the viscosity of oxygen. The temperature dependence of the total thermal conductivity $\lambda(\rho,T)$ results from the thermal conducitivity in the zero-density limit $\lambda_0(T)$ while the density dependence is incorporated in the residual contribution $\Delta\lambda(\rho)$. A third term $\Delta\lambda_c(\rho,T)$ is required to represent the critical enhancement,

$$\lambda(\rho,T) = \lambda_0(T) + \Delta\lambda(\rho) + \Delta\lambda_c(\rho,T). \quad (6)$$

As for the viscosity, the three contributions were evaluated individually and not as a global surface fit. This method would allow for the compensation of deficiencies in one term by the flexibility of another, thus affecting the thermodynamic consistency of the individual contributions.

4.1 Thermal Conductivity in the Zero-Density Limit

In the case of polyatomic molecules the macroscopic thermal conductivity of the dilute gas $\lambda_0(T)$ results from two microscopic energy transfer mechanisms: energy transfer due to translational motion of the molecules and energy transfer via their internal degrees of freedom. Thus, the temperature function of the thermal conductivity in the dilute gas region is constituted according to

$$\lambda_0(T) = \lambda_{tr}(T) + \lambda_{int}(T). \quad (7)$$

The more detailed expression used in this work is an empirically simplified formula based on kinetic theory and the Mason-Monchick approximation as presented by Maitland *et al.*:[40]

$$\lambda_0(T) = \frac{5R}{2M}\eta_0(T)\left\{\frac{3}{2}+d_1\right\}+\frac{R}{M}\eta_0(T)d_2\left\{\frac{c_{v0}(T)}{R}+d_1\right\}, \quad (8)$$

where R is the universal gas constant, M is the molar mass, $\eta_0(T)$ is the viscosity of the dilute gas, Eq. (2), and $c_{v0}(T)$ is the isochoric specific heat capacity of the ideal gas from the IUPAC formulation.[2] The parameters d_1 and d_2 are related to the energy diffusion via internal modes and the rotational collision number, respectively. Their values were determined by a fit of weighted least squares using the low-density data of Keyes,[37] Roder,[35] Geier and Schäfer,[41] Saxena and Gupta,[42] and Jain and Saxena.[43] This yielded

$$d_1 = 1.024\ 506\ 9,\ d_2 = 1.028\ 012\ 7.$$

Figure 9 illustrates the thermal conductivity of dilute oxygen as obtained from Eq. (8) with these values for temperatures from 70 K up to 1400 K. It reveals in addition that the energy transfer through internal degrees of freedom λ_{int} is the predominant contribution while the translational part λ_{tr} amounts only to about 20% of λ_0.

The correlation is compared with fitted and unfitted data sets in Fig. 10 at temperatures up to 500 K. The selected low-density data of Roder[35] show an excellent internal consistency and agree with the low-density data by Keyes[37] within ±1%. The measurements of Johnston and Grilly[44] may be considered also of good internal consistency but exhibit a systematic trend with deviations of −3% on the low end at 130 K and 5.5% at

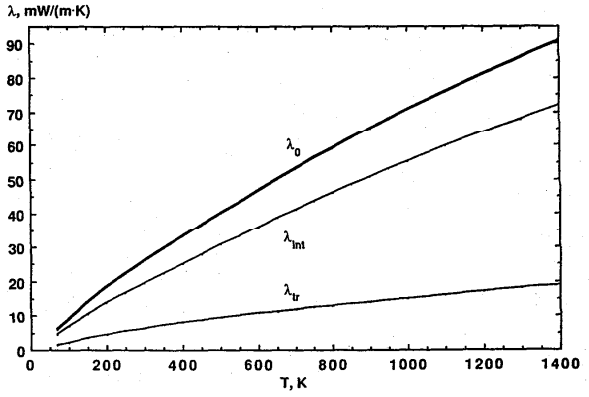

FIG. 9. The thermal conductivity of oxygen at zero density, Eq. (8).

380 K. A similar trend is found in the low-density data of Tsederberg[45] and Ivanova *et al.*[46] with deviations of −4% at 110 K and 6% at 373 K. The data point at 253 K seems to be an outlier in the measurements of Ivanova *et al.* while the data by Pereira and Raw[47] appear to be too high by an average of 2.5%.

Low-density data from previous evaluations which cover only a limited temperature range are compared with the new correlation in Fig. 11 up to 400 K. There is generally good agreement within ±1% above 150 K, and it seems that none of these analyses relied on the previously discussed measurements by Johnston and Grilly, Tsederberg, or Ivanova *et al.* The correlation of Younglove appears unsuitable for extrapolation beyond its upper temperature limit of 400 K since it would yield systematically too high thermal conductivities. Higher discrepancies exist below 150 K where the evaluations differ considerably. Younglove's correlation appears to follow mainly the data by Johnston and Grilly in this range and deviates by as much as −3% at 100 K while the data reported by the Japanese Society of Mechanical Engineers deviate by 8.5% at 90 K. This, however, is not supported by any measurements we are aware of. The earliest evaluation by Vassermann and Rabinovich[48] is supposedly based on Russian data only, reporting values which differ by −1.5% on the average. The data by Hanley, McCarty, and Sengers agree best with the new correlation with deviations of ±0.5%.

While the viscosity of dilute oxygen has been measured up to 2000 K the available thermal conductivity data reach only up to 1600 K. There are five data sets in the high temperature region all of which have been obtained with steady-state hot-wire instruments. Figure 12 shows that the experimental results are inconsistent above 500 K and scatter by roughly ±3%. This is about double the margin which was found for the dilute viscosity data, Fig. 3. The correlation is based in this range on a compromise between the data of Geier and Schäfer[41] and those of Saxena and Gupta[42] which exhibit different trends. A smaller weight was assigned to the measurements of Jain and Saxena[43] since they appear too high at 1500 K and 1600 K. Franck's data[49] are similar to those of Saxena's group whereas the measurements of Westenberg and de Haas[50] range between the remaining data from 700 K to 1000 K. Franck's data agree well with the correlation below room temperature.

Figure 12 includes also the deviations of three previous correlations. Two of them rely exclusively on experimental data with opposite trends. While Touloukian *et al.*[51] rated the measurements of Geier and Schäfer highest, the low density results of Vargaftik *et al.*[52] are close those of Saxena's group above 500 K. The correlation of Hanley and Ely has to be considered separately since it is based on viscosity data only. Nevertheless, these results are clearly too high above 600 K and not confirmed by any experimental information.

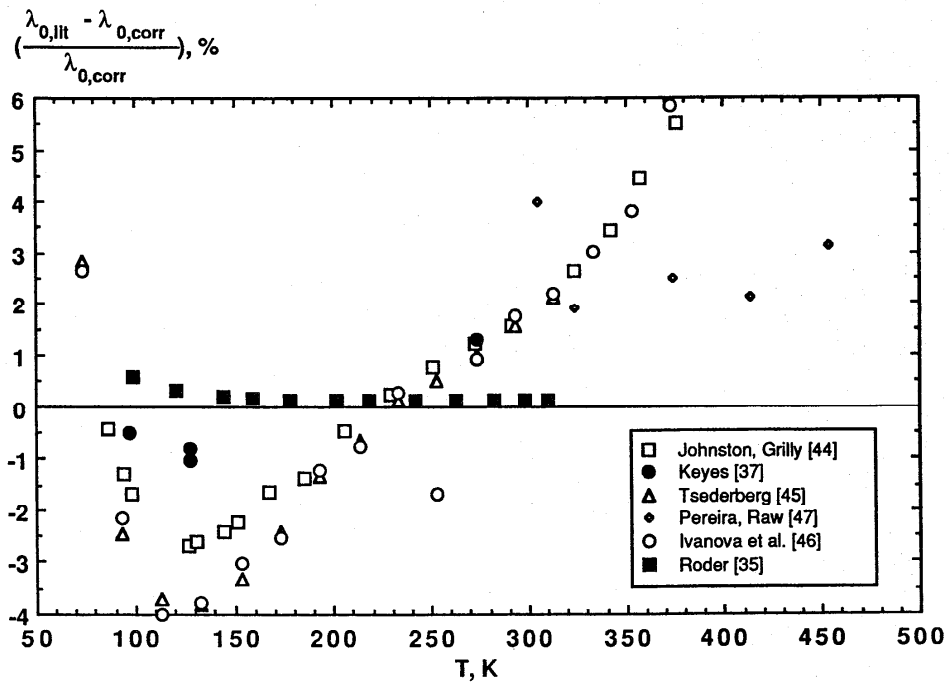

FIG. 10. Percentage deviations of experimental data from the correlation for the thermal conductivity of oxygen at zero density and temperatures up to 500 K.

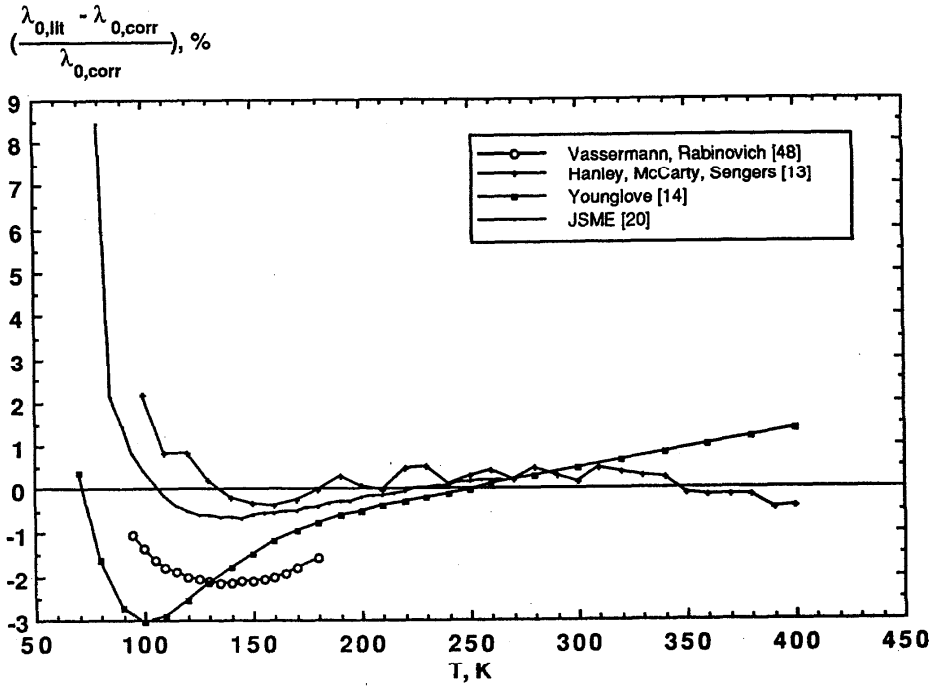

FIG. 11. Percentage deviations of previous evaluations from the correlation for the thermal conductivity of oxygen at zero density and temperatures up to 500 K.

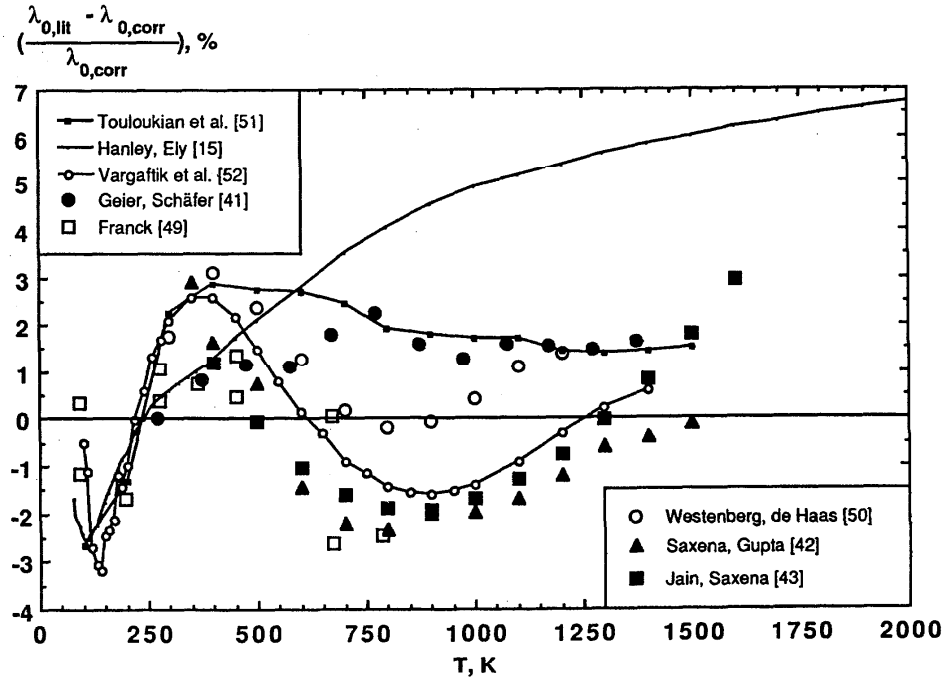

FIG. 12. Percentage deviations of experimental data and previous evaluations from the correlation for the thermal conductivity of oxygen at zero density and temperatures up to 2000 K.

In order to check the consistency of the dilute-gas functions for the viscosity η_0 and thermal conductivity λ_0 of oxygen the Eucken factor $\lambda_0 M/(\eta_0 c_{v0})$ was calculated with M the molar mass and c_{v0} the isochoric heat capacity of the ideal gas as before. The values of this quantity should range for nonpolar gases between the original Eucken factor and the so called modified Eucken factor (cf. Reid *et al.*[53], pp. 493ff.). Figure 13 illustrates that this is also found for oxygen with the "real" Eucken factor close and parallel to the original expression. The correlation of Stiel and Thodos[53] also yields smaller values than the modified expression.

4.2. The Residual Thermal Conductivity

Experimental information on the pressure dependence of the thermal conductivity of oxygen is rather scarce. Only six data sources could be included in this study with a clear preference for the measurements of Roder[35] and to a lesser degree those by Keyes.[37] However, the entire data set of Roder could not be used to correlate the residual thermal conductivity since a critical enhancement of the thermal conductivity was observed in that investigation. Therefore, a subset of 202 data points was selected where the critical enhancement has virtually no influence. Since the residual thermal conductivity is typically less density-dependent than the residual viscosity it can be represented by polynomial expressions. The dimensionless form,

$$\frac{\Delta\lambda(\rho)}{\Lambda} = \sum_{i=1}^{5} e_i \cdot \rho_R^i, \tag{9}$$

in terms of the reduced density $\rho_R = \rho/\rho_c$ was chosen here. Omitting an absolute term ensures the proper transition of the function to the zero-density limit. The parameter values for an optimal representation of the selected data were obtained from a least-squares fit as follows:

$$e_1 = 2.328\ 250\ 85, \quad e_2 = 4.230\ 242\ 31,$$
$$e_3 = -3.607\ 983\ 07, \quad e_4 = 2.016\ 756\ 31,$$
$$e_5 = -0.289\ 731\ 736.$$

It is inappropriate to employ the thermal conductivity value at the critical point as a reduction constant in dimensionless expressions. In analogy to the viscosity correlation we used therefore the entity

$$\Lambda = \frac{R^{5/6} p_c^{2/3}}{T_c^{1/6} M^{1/2} N_A^{1/3}} = \frac{k^{5/6} p_c^{2/3}}{T_c^{1/6} m^{1/2}} = H \cdot \frac{R}{M} = H \cdot \frac{k}{m} \tag{10}$$

as a substance-characteristic thermal conductivity factor. Λ is related to the viscosity factor H as indicated above and yields a value of 4.909 mW/(m·K) for oxygen. This value, however, does not match a point on the thermal conductivity surface of oxygen.

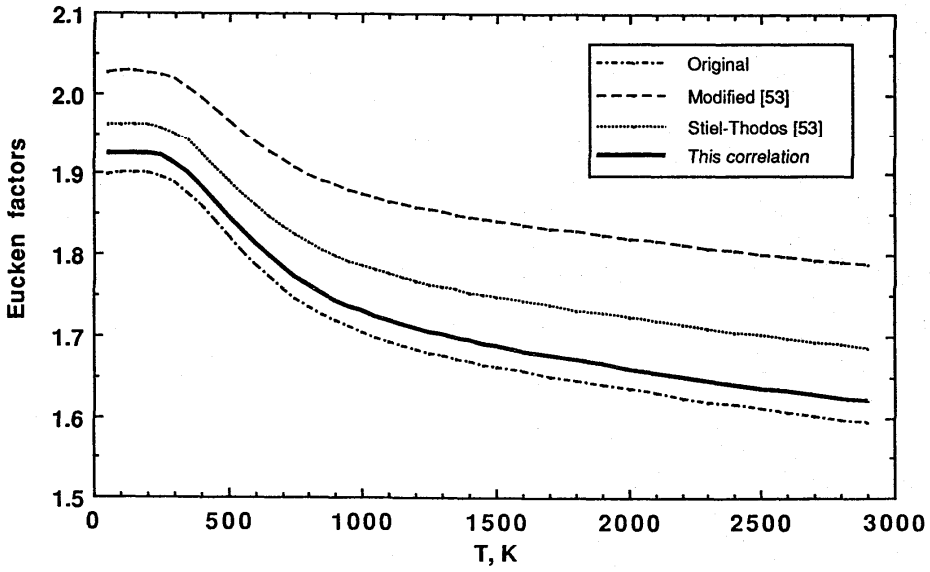

FIG. 13. Comparison of the Eucken factors.

The residual thermal conductivity is shown in Fig. 14 as a function of density according to Eq. (9). The accuracy of the new correlation in comparison with the selected data is shown in Fig. 15. These comparisons are made on the basis of the total thermal conductivity $\lambda_0(T) + \Delta\lambda(\rho)$ rather than only the residual thermal conductivity $\Delta\lambda(\rho)$. Three regions can be distinguished in the diagram. Up to 5 mol/L, the data of Roder[35] exhibit some systematic trends but are reproduced within ±2%. The agreement is well within ±1% at densities up to 26 mol/L where the data which reflect a critical enhancement have been removed. Further, the deviations become systematic with maxima of ±3% due to an additional weak temperature dependence of the thermal conductivity. The overall representation of Roder's data is excellent with an average deviation of 0.03% and a standard deviation of ±1% which is smaller than the quoted experimental accuracy of ±1.5%.

Figure 15 shows also the representation of Roder's data when his expression for the residual thermal conductivity is used instead of Eq. (9). The deviations diminsh almost entirely due to the additional temperature polynomials in Roder's correlation. However, these temperature functions may fail when extrapolated beyond the range of the data on which they are based. Therefore, we decided to retain a temperature independent formulation of the residual thermal conductivity.

A comparison of the earlier measurements with the new correlation is presented in Fig. 16 reflecting the data situation until Roder's measurements became available. Most of these data are higher than the correlation up to a density of 14 mol/L. Probably this is a result of convection effects since steady-state methods were used in these studies. While the data of Tsederberg[45] and Ivanova *et al.*[46] reach maximum deviations of about 10% around 6 mol/L, the data by Ziebland and Burton[38] exhibit discrepancies of as much as 24% in that density range. The results by Ziebland and Burton seem also too high between 20 and 24 mol/L as opposed to the data of Borovik,[39] which deviate by −12% in that region. That these discrepancies are partly due to a critical enhancement cannot be ruled out. Better agreement exists above 25 mol/L where the literature data scatter in a ±2% band with a slight tendency to negative deviations as the density increases but not exceeding −5%. An additional temperature dependence is observed there in the data of Tsederberg but the trend is the opposite of that found by Roder. The 73 K isotherm of Ivanova *et al.* is consistently 7.5% lower than the correlation.

Table 2 presents further information about the agreement of previously evaluated data with the new correlation. The earliest analysis of the thermal conductivity of oxygen was carried out by Vassermann and Rabinovich[48] in 1970 for yet a limited temperature and pressure range. The results, however, agree favorably with the present correlation and deviate only by at most 6% and −3%, respectively. The later correlation by Hanley, McCarty, and Sengers[13] is based exclusively on the measurements of Ziebland and Burton which from Fig. 16 appear to be seriously influenced by convection. Consequently, the evaluated data by Hanley, McCarty, and Sengers yield discrepancies of up to 37% when compared with the new correlation. The data set from the exhaustive thermal conductivity compilation by Vargaftik *et al.*[52] is in good agreement with the new correlation when judged by the average deviation of only 1.1%. A more detailed inspection reveals, however, that these data are systematically too high at intermediate densities around 15 mol/L while negative deviations of down to −9.5% occur above 28 mol/L. The effect of the critical enhancement cannot be the reason for the discrepancies since the deviations range only between 6% and −1.6% along the near-critical 5 MPa isobar.

Comparisons with the most recent compilations by Younglove[14] and by the Japanese Society of Mechanical Engineers[20] are presented in Figs. 17 and 18, respectively. Unlike the tabulated data of Younglove, the comparison does not include the critical enhancement of the thermal conductivity. The background thermal conductivity was calculated from Younglove's correlations (including densities from the modified BWR equation of state) which are part of the widely used MIPROPS package.[54] The calculated values yield a rather small average deviation of −0.5% but its standard deviation of 6.9% and the extreme deviations of 21.3% and −28.9%, respectively, indicate systematic discrepancies. They are illustrated in Fig. 17 along five isobars. The positive deviations occur close to the saturation boundary in the subcritical gas region but are flattening out to higher temperatures. The negative deviations from too small thermal conductivities increase with pressure to values which are clearly beyond the uncertainty of the experimental data.

Similar trends result from the comparison with the data set of JSME, Fig.18, which refers only to subambient temperatures. The deviations range mostly in a ±15% band with the exception of the 5 MPa isobar where the positive deviations close to the dew line reach a maximum of 65%. A close inspection of the data set brought no evidence that this extreme would be due to a critical enhancement. The maximum appears also on supercritical isobars but flattens out eventually at the highest pressure of 35 MPa. The deviation lines show also a systematic step between 105 K and 110 K where the data set seems to be not smooth.

Thermal conductivity values which were calculated from the newly established correlation are presented in Table 3 for the saturation boundary and in Table 5 for the entire fluid region in a pressure range from 0.1 to 100 MPa and for temperatures from 70 to 1400 K.

4.3. The Critical Enhancement of the Thermal Conductivity

Oxygen is one of the fluids for which an enhancement of the thermal conductivity in the critical region is experimentally confirmed. However, only the most recent investigations of Roder[35] and Weber[36] have revealed this

TABLE 5. Thermal conductivity (mW/(*m*·K)) of oxygen

p, MPa \ *T*, K	70	80	90	100	110	120	130	140	150	160	170	180
0.1	181.0	166.9	152.8	9.297	10.31	11.31	12.28	13.22	14.15	15.05	15.94	16.80
1	181.4	167.4	153.4	139.4	125.1	12.37	13.20	14.04	14.89	15.73	16.56	17.38
2	181.9	168.0	154.1	140.2	126.1	111.5	95.85	15.45	16.05	16.74	17.46	18.19
3	182.4	168.5	154.8	141.0	127.1	112.8	97.59	80.10	17.85	18.14	18.63	19.21
4	182.8	169.1	155.4	141.8	128.0	113.9	99.22	82.83	21.42	20.19	20.18	20.48
5	183.3	169.6	156.0	142.5	128.9	115.1	100.8	85.20	65.57	23.68	22.29	22.08
6	183.8	170.1	156.7	143.3	129.8	116.2	102.2	87.32	69.98	34.60	25.35	24.10
7	184.2	170.7	157.3	144.0	130.7	117.3	103.6	89.26	73.33	51.90	30.16	26.69
8	184.7	171.2	157.9	144.7	131.6	118.3	104.9	91.04	76.12	58.48	37.57	30.02
9	185.1	171.7	158.5	145.5	132.4	119.4	106.2	92.71	78.55	62.87	45.18	34.14
10	185.6	172.3	159.1	146.2	133.3	120.4	107.4	94.29	80.73	66.31	50.90	38.77
15	187.8	174.8	162.1	149.5	137.2	125.0	113.0	101.1	89.41	77.92	66.87	56.80
20	189.9	177.2	164.9	152.7	140.9	129.2	117.9	106.8	96.11	85.87	76.25	67.48
25	192.0	179.6	167.5	155.8	144.3	133.1	122.3	111.8	101.8	92.26	83.40	75.31
30	194.0	181.9	170.1	158.6	147.5	136.7	126.3	116.3	106.7	97.74	89.37	81.71
35	196.0	184.1	172.5	161.4	150.6	140.1	130.0	120.4	111.2	102.6	94.59	87.24
40	197.9	186.2	174.9	164.0	153.5	143.3	133.5	124.2	115.3	107.0	99.28	92.16
45	199.8	188.3	177.2	166.5	156.2	146.3	136.8	127.7	119.2	111.1	103.6	96.63
50	201.6	190.3	179.4	169.0	158.9	149.2	139.9	131.1	122.7	114.9	107.5	100.8
60		194.1	183.7	173.6	163.9	154.6	145.7	137.3	129.3	121.8	114.7	108.2
70		197.8	187.6	177.9	168.6	159.6	151.1	143.0	135.2	128.0	121.2	114.9
80		201.3	191.4	182.0	173.0	164.3	156.0	148.2	140.7	133.7	127.1	120.9
90		204.6	195.0	185.9	177.1	168.7	160.7	153.0	145.8	139.0	132.5	126.5
100			198.4	189.5	181.0	172.8	165.0	157.6	150.5	143.9	137.6	131.6

p, MPa \ *T*, K	190	200	220	240	260	280	300	320	340	360	380	400
0.1	17.65	18.48	20.10	21.67	23.20	24.69	26.15	27.60	29.03	30.44	31.85	33.24
1	18.19	18.99	20.56	22.08	23.57	25.03	26.47	27.90	29.31	30.71	32.10	33.48
2	18.93	19.68	21.15	22.61	24.04	25.46	26.87	28.26	29.65	31.02	32.39	33.76
3	19.84	20.49	21.84	23.20	24.57	25.94	27.30	28.66	30.01	31.36	32.71	34.06
4	20.93	21.45	22.62	23.87	25.15	26.46	27.77	29.08	30.40	31.73	33.05	34.37
5	22.23	22.57	23.50	24.60	25.79	27.01	28.27	29.54	30.82	32.11	33.40	34.71
6	23.80	23.86	24.48	25.41	26.47	27.61	28.80	30.01	31.25	32.51	33.78	35.05
7	25.66	25.35	25.57	26.28	27.20	28.24	29.36	30.52	31.71	32.93	34.16	35.41
8	27.87	27.04	26.76	27.21	27.98	28.91	29.94	31.04	32.19	33.36	34.56	35.78
9	30.43	28.93	28.04	28.20	28.79	29.61	30.55	31.59	32.68	33.81	34.98	36.17
10	33.34	31.03	29.42	29.25	29.65	30.33	31.19	32.15	33.18	34.27	35.40	36.56
15	48.68	43.05	37.32	35.12	34.36	34.29	34.62	35.18	35.90	36.74	37.66	38.65
20	59.86	53.68	45.57	41.45	39.45	38.56	38.29	38.42	38.81	39.37	40.07	40.86
25	68.14	62.02	53.01	47.61	44.55	42.87	42.04	41.73	41.77	42.06	42.54	43.14
30	74.85	68.85	59.51	53.31	49.44	47.10	45.73	45.01	44.73	44.76	45.01	45.43
35	80.60	74.72	65.24	58.55	54.07	51.16	49.33	48.23	47.64	47.41	47.46	47.70
40	85.69	79.91	70.38	63.36	58.42	55.05	52.81	51.36	50.49	50.02	49.86	49.93
45	90.31	84.61	75.06	67.81	62.53	58.77	56.17	54.41	53.26	52.57	52.22	52.13
50	94.55	88.92	79.38	71.97	66.40	62.33	59.42	57.37	55.98	55.07	54.53	54.28
60	102.2	96.68	87.17	79.55	73.58	69.02	65.59	63.05	61.21	59.91	59.03	58.48
70	109.0	103.6	94.12	86.37	80.13	75.20	71.37	68.43	66.21	64.56	63.36	62.53
80	115.1	109.8	100.4	92.60	86.17	80.97	76.82	73.54	70.99	69.03	67.56	66.47
90	120.8	115.6	106.2	98.36	91.78	86.37	81.97	78.42	75.59	73.36	71.62	70.30
100	126.1	120.9	111.6	103.7	97.05	91.47	86.85	83.07	80.00	77.53	75.57	74.03

TABLE 5. Thermal conductivity (mW/(m·K)) of oxygen — Continued

p, MPa	T, K 420	440	460	480	500	550	600	650	700	750	800	850
0.1	34.63	36.01	37.38	38.74	40.10	43.45	46.73	49.94	53.09	56.15	59.15	62.08
1	34.85	36.22	37.59	38.94	40.29	43.62	46.89	50.09	53.22	56.28	59.27	62.19
2	35.12	36.48	37.83	39.17	40.51	43.81	47.07	50.25	53.37	56.42	59.40	62.31
3	35.40	36.74	38.08	39.41	40.74	44.02	47.25	50.42	53.53	56.57	59.53	62.44
4	35.70	37.02	38.34	39.66	40.98	44.23	47.45	50.60	53.69	56.72	59.67	62.57
5	36.01	37.32	38.62	39.92	41.23	44.46	47.65	50.78	53.86	56.87	59.82	62.70
6	36.33	37.62	38.91	40.20	41.48	44.69	47.85	50.97	54.03	57.03	59.97	62.84
7	36.67	37.93	39.20	40.48	41.75	44.92	48.06	51.16	54.21	57.19	60.12	62.98
8	37.02	38.26	39.51	40.77	42.02	45.16	48.28	51.36	54.38	57.36	60.27	63.12
9	37.37	38.59	39.82	41.06	42.30	45.41	48.50	51.56	54.57	57.52	60.42	63.27
10	37.74	38.94	40.15	41.37	42.59	45.66	48.73	51.76	54.75	57.70	60.58	63.41
15	39.68	40.75	41.84	42.96	44.10	46.99	49.91	52.83	55.73	58.59	61.41	64.18
20	41.74	42.67	43.65	44.66	45.71	48.40	51.17	53.96	56.76	59.54	62.28	64.99
25	43.85	44.65	45.50	46.41	47.36	49.85	52.47	55.14	57.83	60.51	63.19	65.83
30	45.98	46.64	47.37	48.18	49.03	51.33	53.79	56.33	58.91	61.51	64.11	66.69
35	48.10	48.62	49.24	49.94	50.70	52.81	55.11	57.53	60.01	62.53	65.05	67.56
40	50.19	50.58	51.09	51.69	52.36	54.28	56.44	58.73	61.12	63.54	65.99	68.44
45	52.24	52.51	52.91	53.41	54.00	55.74	57.75	59.93	62.22	64.56	66.94	69.32
50	54.26	54.41	54.70	55.11	55.61	57.18	59.05	61.12	63.31	65.57	67.88	70.20
60	58.19	58.11	58.20	58.43	58.77	60.00	61.61	63.46	65.46	67.57	69.74	71.95
70	62.00	61.70	61.60	61.66	61.85	62.75	64.10	65.74	67.57	69.53	71.57	73.67
80	65.71	65.20	64.91	64.80	64.84	65.43	66.53	67.97	69.63	71.44	73.36	75.35
90	69.32	68.62	68.15	67.88	67.77	68.05	68.91	70.14	71.64	73.32	75.12	77.01
100	72.84	71.96	71.32	70.89	70.64	70.62	71.24	72.28	73.62	75.16	76.84	78.63

p, MPa	T, K 900	950	1000	1100	1200	1300	1400
0.1	64.94	67.73	70.47	75.79	80.93	85.91	90.78
1	65.04	67.83	70.57	75.88	81.01	85.98	90.84
2	65.16	67.94	70.67	75.97	81.09	86.06	90.92
3	65.28	68.06	70.78	76.07	81.18	86.15	90.99
4	65.40	68.17	70.89	76.17	81.27	86.23	91.07
5	65.53	68.29	71.00	76.27	81.36	86.31	91.14
6	65.65	68.41	71.11	76.37	81.46	86.40	91.22
7	65.78	68.53	71.23	76.48	81.55	86.48	91.30
8	65.92	68.66	71.35	76.58	81.65	86.57	91.38
9	66.05	68.79	71.47	76.69	81.74	86.66	91.47
10	66.19	68.92	71.59	76.80	81.84	86.75	91.55
15	66.91	69.59	72.22	77.36	82.35	87.22	91.98
20	67.66	70.30	72.89	77.96	82.89	87.71	92.42
25	68.45	71.03	73.58	78.57	83.45	88.21	92.89
30	69.25	71.78	74.29	79.21	84.02	88.73	93.37
35	70.07	72.55	75.01	79.85	84.60	89.26	93.85
40	70.89	73.32	75.73	80.50	85.19	89.80	94.35
45	71.71	74.10	76.47	81.16	85.79	90.35	94.85
50	72.54	74.87	77.20	81.82	86.39	90.89	95.35
60	74.18	76.42	78.67	83.14	87.59	92.00	96.37
70	75.80	77.96	80.12	84.46	88.79	93.10	97.39
80	77.39	79.46	81.55	85.76	89.98	94.20	98.41
90	78.95	80.94	82.96	87.04	91.15	95.28	99.41
100	80.48	82.39	84.34	88.30	92.31	96.35	100.4

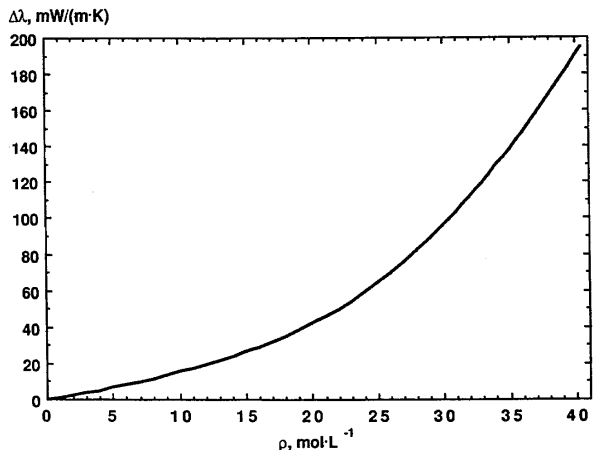

FIG. 14. The residual thermal conducitvity of oxygen, Eq. (9).

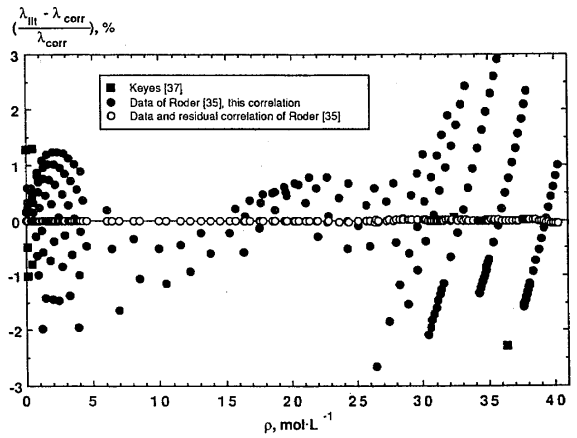

FIG. 15. Percentage deviations of the selected data sets from the correlation for the thermal conductivity of oxygen.

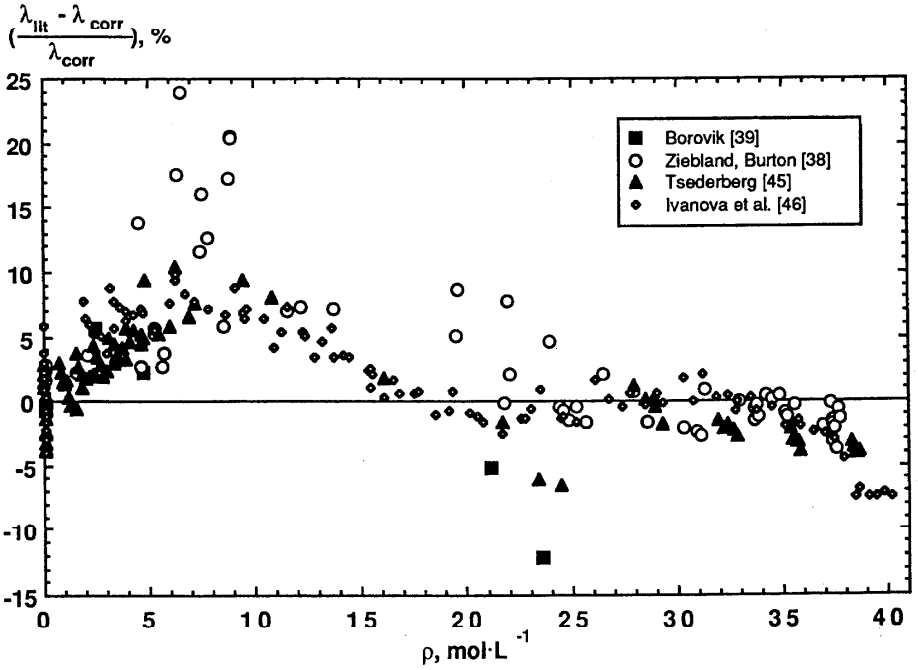

FIG. 16. Percentage deviations of data sets which were not selected from the correlation for the thermal conductivity of oxygen.

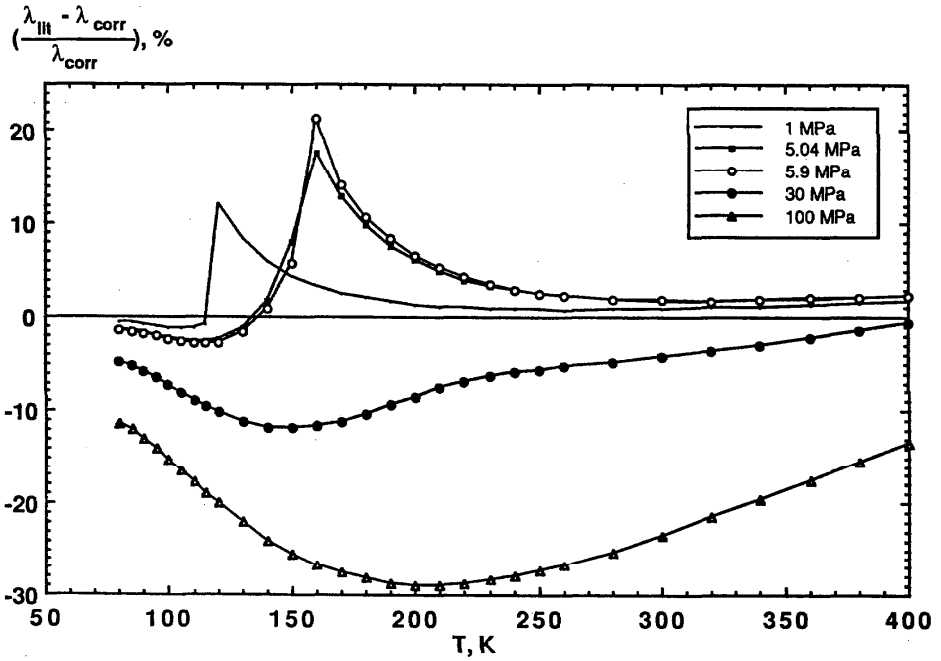

FIG. 17. Percentage deviations of the correlation of Younglove[14] from the correlation for the thermal conductivity of oxygen.

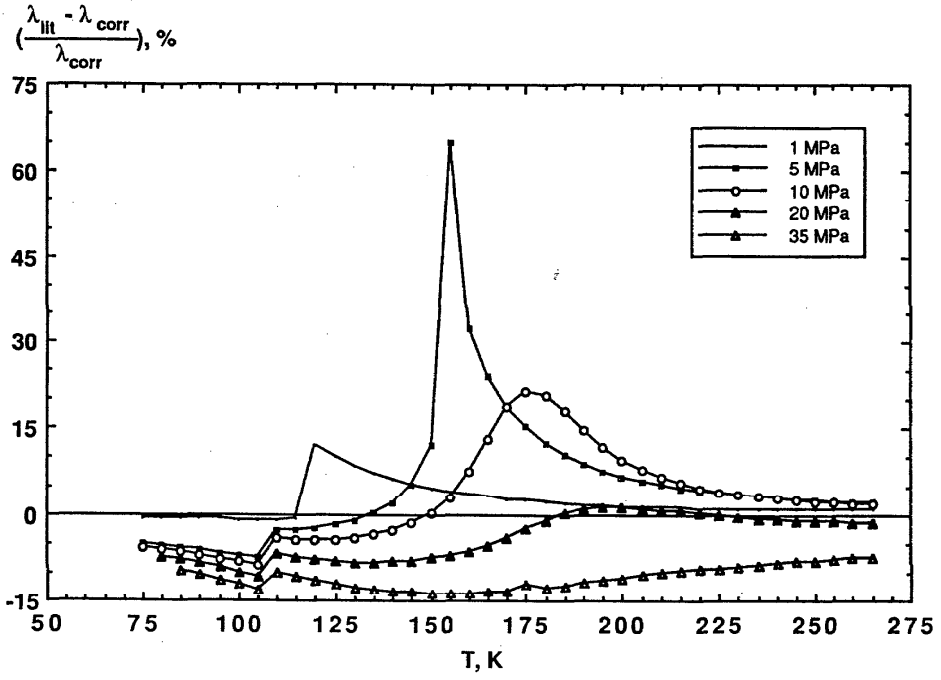

FIG. 18. Percentage deviations of the data set of JSME[20] from the correlation for the thermal conductivity of oxygen.

behavior, which was not found in the earlier measurements. These two studies provide quite detailed information since the immediate vicinity of the critical point was investigated with two different experimental methods. Roder's data were obtained by the transient hot-wire method whereas Weber used a Rayleigh light scattering technique which allows measurements of the thermal diffusivity under macroscopic equilibrium. Weber, however, failed to report the original experimental information and listed instead thermal conductivity data which were derived from the thermal diffusivities using density and specific isobaric heat capacity values.

The magnitude of the critical enhancement is illustrated in Fig. 19 which displays the entire data set of Roder and the 76 data points of Weber. The thermal conductivities of Weber range up to 26 times higher than the background values. To visualize the enhancement as obtained by Roder with higher resolution, percentage deviations between these data and the values calculated from the present correlation are shown in Fig. 20. The enhancement amounts only to a factor of 1.5 relative to the background contribution because Roder did not measure in such a proximity to the critical point as did Weber. The loci of Weber's measurements are shown in the density-temperature plane, Fig. 21, together with the saturation boundary as given by the IUPAC formulation. All data along the saturation boundary in fact do fall inside the two phase region. Although rather small, this superheating or subcooling leads to significant consequences in the present correlation of the data.

While Weber attempted only a description of his data on a theoretical basis, Roder developed a quite accurate semiempirical correlation for his results. The comparison with the data set of Weber left some unresolved discrepancies[33] at densities considerably different from the critical density. The critical enhancement of the thermal conductivity is closely coupled to the density and the isobaric specific heat capacity of a fluid, and the IUPAC fundamental equation of state represents a remarkable progress in the description of these equilibrium properties particularly in the critical region. Therefore, the densities which correspond to the pressures and temperatures as measured by Roder were recalculated from the IUPAC formulation and compared with Roder's tabulated values which were obtained from the modified BWR equation of state. Ten data points (labeled 17084 through 17093 in Roder's work) represent liquid or two phase states where the liquid is superheated by up to 2.3 K. Other than that, the density differences are generally small but become significant in the vicinity of the critical point. Fig. 22 shows these deviations which amount to maxima of 3.7% and −3%, respectively. The systematic trend of the deviations has been found similarly in other comparisons between the modified BWR and the Schmidt-Wagner equation of state.[55] Interestingly, Roder's correlation of the critical enhancement produced the highest deviations just for these data points.

The consistency of Weber's density measurements cannot be checked since no information about the associ-

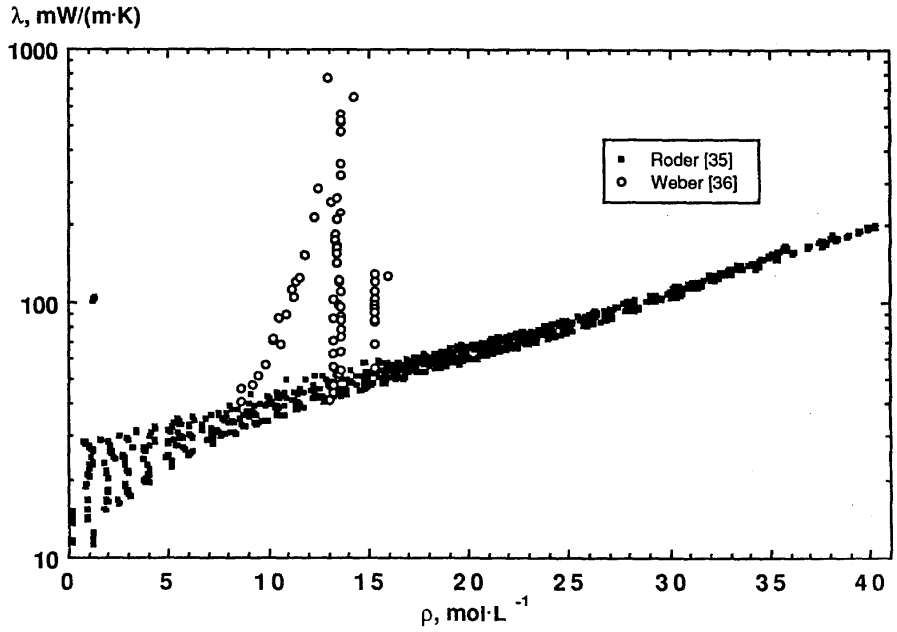

FIG. 19. Experimental data of Roder[35] and Weber[36] for the thermal conductivity of oxygen.

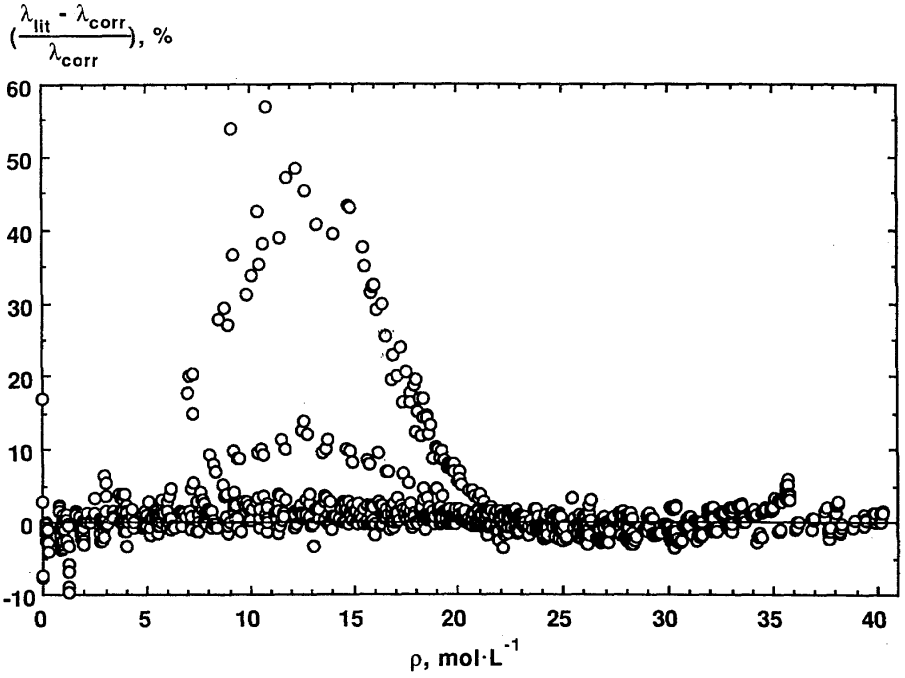

FIG. 20. The enhancement of the thermal conductivity of oxygen in the critical region based on the data set of Roder[35] compared with the correlation.

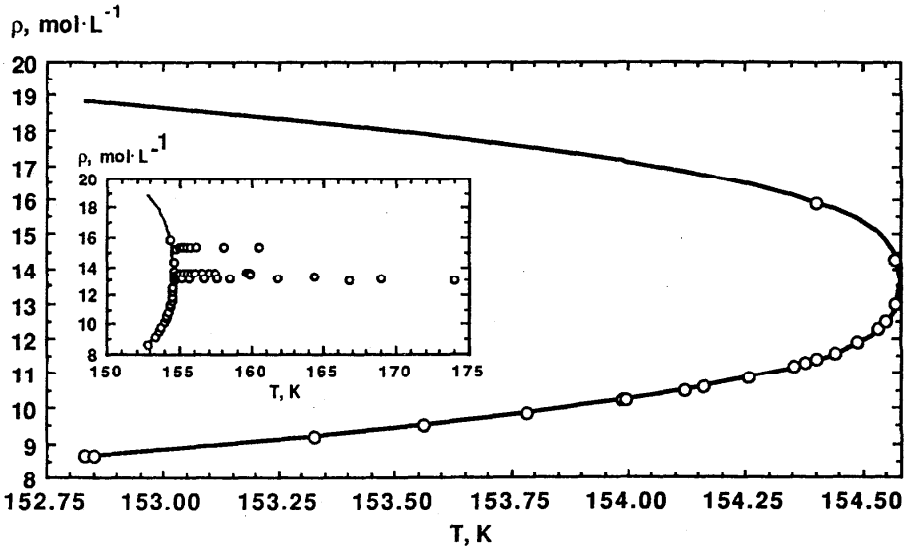

FIG. 21. Distribution of the thermal diffusivity measurements of Weber[36] in the density-temperature plane. All data in the large scale diagram are inside the saturation boundary as calculated from the IUPAC equation of state. Inset shows distribution of the entire data set.

ated pressures is provided. To convert the measured thermal diffusivities to thermal conductivities Weber used c_p-values from the scaled equation of state, a polynomial representation of the critical isochore, and the modified BWR equation of state along the saturation boundary.[36] The influence of c_p on the representation of the critical thermal conductivity enhancement may be assesed by the comparison illustrated in Fig. 23. The c_p values for the data points of Weber as obtained from the IUPAC formulation and the modified BWR equation of state are plotted on an absolute scale. In the extreme the values differ by a factor of 19. The IUPAC formulation yields negative heat capacities in four cases because some data points of Weber are located within the two-phase region.

There are three choices to represent the critical enhancement of the thermal conductivity. In order to achieve a high accuracy one may use a semiempirical correlation like Roder's. It requires seven adjustable parameters and may not be applicable to other fluids without modifications. On the other hand, the complete solution of the mode-coupling equations for the dynamics of critical fluctuations including the crossover from the singular to the regular behavior of the transport properties as outlined by Olchowy and Sengers[56] is a universal representation but requires an extensive amount of programming and execution time. In between these methods ranges the simplified crossover model which was presented recently by Olchowy and Sengers.[57] It retains the universality of the complete solution at a reduced complexity, requires only one adjustable parameter per fluid, and appears therefore more suitable for engineering purposes. In terms of the simplified crossover model the critical enhancement of the thermal conductivity is expressed as

$$\Delta\lambda_c(\rho,T) = \rho\, c_p \frac{R_L k T}{6\pi\eta(\rho,T)\xi}(\Omega-\Omega_0), \tag{11}$$

where ρ, c_p and $\eta(\rho,T)$ are the density, isobaric heat capacity and viscosity of the fluid, k is Boltzmann's constant and $R_L = 1.01 \pm 0.04$ a universal amplitude. With the isochoric heat capacity c_v the terms

$$\Omega = \frac{2}{\pi}\left[\left(\frac{c_p-c_v}{c_p}\right)\mathrm{arctg}(q_{D,av}\xi) + \frac{c_v}{c_p}q_{D,av}\xi\right] \tag{12}$$

and

$$\Omega_0 = \frac{2}{\pi}\left\{1-\exp\left[-\frac{1}{\frac{1}{q_{D,av}\xi}+\frac{1}{3}\left(\frac{\rho_c}{\rho}q_{D,av}\xi\right)^2}\right]\right\} \tag{13}$$

result from the approximation of the mode-coupling integral equations and include the effective cutoff $q_{D,av}$ as the one fluid-dependent parameter which is treated as a constant. The correlation length ξ is related via the power law

$$\xi = \xi_0\left(\frac{\Delta\chi}{\Gamma}\right)^{\frac{\nu}{\gamma}} \tag{14}$$

to the amplitudes $\xi_0 = 0.16$ nm and $\Gamma = 0.083\,91$ with the critical exponents $\nu = 0.63$ and $\gamma = 1.2415$. The difference

$$\Delta\chi = \chi(\rho,T) - \frac{T_{ref}}{T}\chi(\rho,T_{ref}) \tag{15}$$

of the reduced compressibilities

$$\chi(\rho,T) = \frac{p_c}{\rho_c^2}\frac{\rho}{\left(\frac{\partial p}{\partial\rho}\right)_T} \tag{16}$$

is taken between the actual state point (ρ,T) and a state point at the same density but a reference temperature $T_{ref} = 2\,T_c$ far above the critical temperature T_c. Reducing parameters are the critical pressure p_c and the critical density ρ_c.

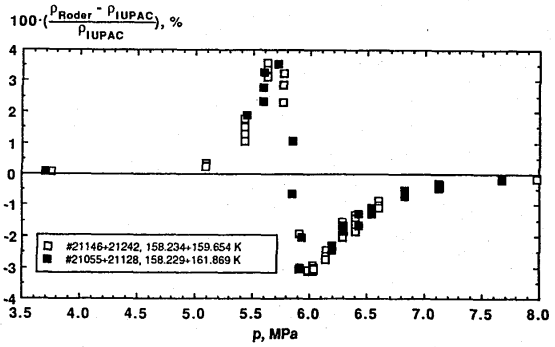

FIG. 22. Percentage deviations between the densities of Roder[35] and values calculated from the IUPAC equation of state.

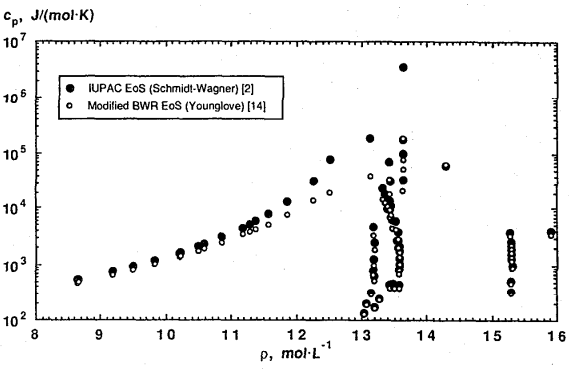

FIG. 23. Comparison of specific isobaric heat capacities as calculated from the IUPAC equation of state[2] and the modified BWR equation of state[14] for the data of Weber[36].

To test the suitability of this model a subset of 104 points was selected from Roder's measurements for which the deviation from the background thermal conductivity according to Eqs. (8) and (9) exceeded 4%. Using ρ, c_p, and c_v values from the IUPAC formulation and calculating the viscosity from Eqs. (2) and (4), the cutoff length $q_{D,av}^{-1}$ was varied in a parametric study. The quality of the representation is illustrated in Fig. 24 by the dependence of the average deviation Δ_{av} and its standard deviation s as well as the extreme deviations Δ_{max} and Δ_{min} on $q_{D,av}^{-1}$. The model overestimates the thermal conductivity right at the critical point if $q_{D,av}^{-1}$ is chosen so that the tails of the peak flatten out properly to the regular behavior. The corresponding value of $q_{D,av}^{-1}$ = 0.4167 nm is derived from the condition $\Delta_{av} \approx 0$ with calculated thermal conductivities at the most 15% higher than the experimental data. An accurate description of the singularity ($\Delta_{min} \approx 0$) would be achieved by increasing $q_{D,av}^{-1}$ to 0.67 nm, but the thermal conductivity far away from the critical point would be reproduced considerably too high.

The parametric study of $q_{D,av}^{-1}$ was conducted also for a subset of Weber's data. Four values were omitted for which the IUPAC formulation yielded negative heat capacities as well as two other points for which deviations of more than 100% prevailed consistently. As documented in Fig. 25 the representation of Weber's data is much worse with almost constant extreme deviations of −47% and 34% to 48%, respectively. The standard deviation of ±13% is over three times higher than the one obtained for Roder's data. The average deviation becomes zero at $q_{D,av}^{-1} \approx 0.35$ nm which differs also from the previously determined value.

Percentage deviations between the subset of thermal conductivities from Roder's measurements and the calculated values from Eqs. (8), (9), and (11) are shown more detailed in Fig. 26 for $q_{D,av}^{-1}$ = 0.4167 nm. The magnitude of the deviations and their pattern indicate that the simplified crossover model as applied in this work performs comparably well like Roder's semiempirical correlation. With both methods the peak thermal conductivity is overestimated by about 15%. The comparison of the simplified crossover model and that value of $q_{D,av}^{-1}$ with Weber's measurements, Fig. 27, suggests at first that the data are of inferior internal consistency. Their scatter below 13 mol/L is about ±10%, which is the claimed experimental uncertainty. Excluding an apparent outlier, the data in the immediate critical region between 13 and 14 mol/L are represented fairly well with a widening range of deviations from −20% to 15%. As was noted by Weber, the data on the isochore 15.3 mol/L and above are in systematic disagreement, also with the simplified crossover model.

Again, these evaluations were made using the IUPAC formulation for the required thermodynamic properties. The performance of the simplified crossover model would be improved by use of a scaled equation of state in the vicinity of the critical point. However, considering the improvement of the IUPAC formulation over the equation of state information which was used by Roder and Weber and taking into account the substantial experimental uncertainty of thermal conductivity measurements in the critical region, the simplified crossover model with a cutoff length of $q_{D,av}^{-1}$ = 0.4167 nm provides a good representation of the critical enhancement. Figure 28 illustrates the contribution of the critical enhancement term $\Delta\lambda_c$ to the total thermal conductivity in the pressure-temperature plane.

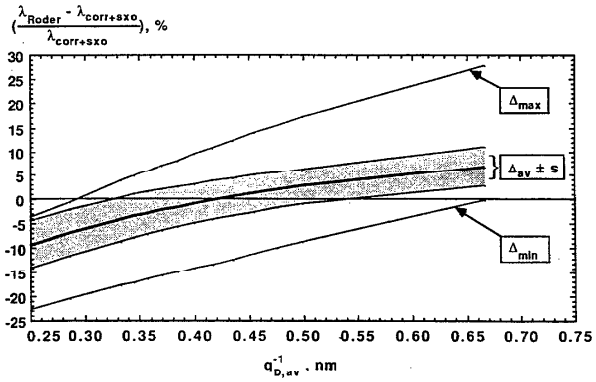

FIG. 24. Percentage deviations between the extracted thermal conductivity data of Roder[35] and values calculated from the correlation with the simplified crossover model and variable cutoff parameter $q_{D,av}^{-1}$.

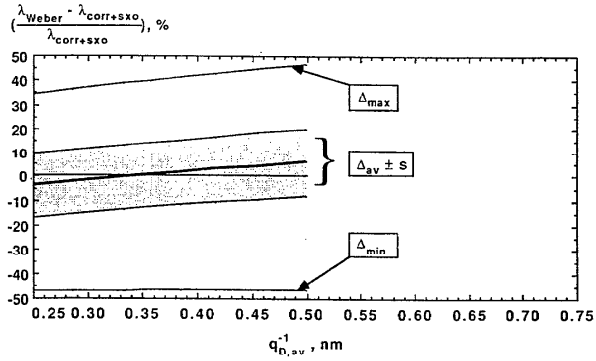

FIG. 25. Percentage deviations between the extracted thermal conductivity data of Weber[36] and values calculated from the correlation with the simplified crossover model and variable cutoff parameter $q_{D,av}^{-1}$.

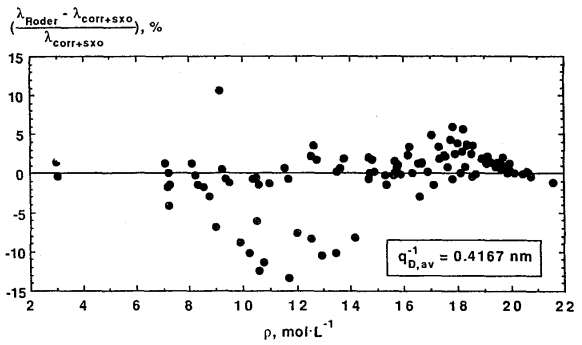

FIG. 26. Percentage deviations between the extracted thermal conductivity data of Roder[35] and values calculated from the correlation with the simplified crossover model.

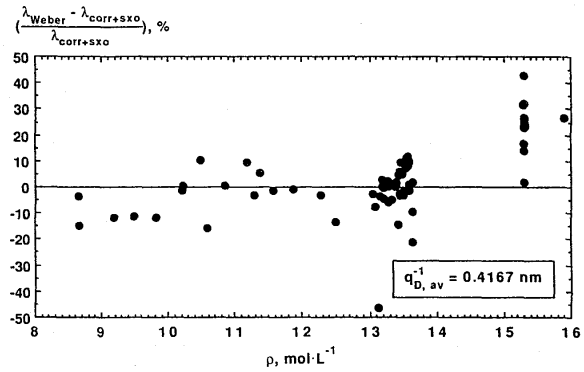

FIG. 27. Percentage deviations between the extracted thermal conductivity data of Weber[36] and values calculated from the correlation with the simplified crossover model.

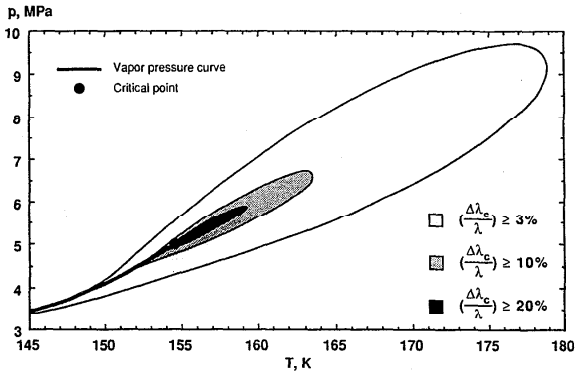

FIG. 28. Contribution of the critical enhancement $\Delta\lambda_c$ to the total thermal conductivity of oxygen.

5. Transport Equations of State for Oxygen

We have developed transport equations of state as an alternate means to describe transport properties directly in terms of pressure and temperature instead of using density and temperature as independent variables. Such a representation is particularly useful for the immediate evaluation of measurements since pressure and temperature are usually the experimentally observed variables. No equation of state is necessary for the data correlation, which may introduce additional uncertainties, unless the working equation of an experiment requires such information.

The formulation of transport equations of state is based on a phenomenological study of viscosity and thermal conductivity surfaces not including critical enhancement effects. Such an analysis suggests that it is advantageous to express the pressure as a function of temperature and transport property, $p = f(T,TP)$. This conclusion may appear trivial since the transport properties depend mainly on the density which is related to pressure and temperature in a similar way known as thermal equations of state, $p = f(T,\rho)$. Nevertheless, it is not possible to simply replace the density in a thermal equation of state by one of the transport properties, nor can the formulation of the transport equation of state be based on a theoretical derivation. Even if one would express the density as a function of the residual transport property, for example $\rho = f(\Delta\eta)$ or $\rho = f(\Delta\lambda)$ by inverting Eqs. (4) and (9), the density could not be replaced in the thermal equation of state without also modifying the temperature functions.

We therefore decided to develop the functional form of the transport equations of state empirically from scratch. The first application was a representation of the viscosity of water within its tolerances assigned by IAPS.[58] A more compact form with 21 adjustable parameters was found for fluids with less complex viscosity and thermal conductivity surfaces. The transport properties of oxygen,[59] nitrogen,[60] and fourteen other fluids[61] could be represented well within the estimated uncertainties of the data. In the dimensionless form $p_R = f(T_R,TP_R)$ with $p_R = p/p_c$ and $T_R = T/T_c$ it turned out useful to transform the transport properties according to

$$TP_R = \ln\left(\frac{TP}{TP^*} + 1\right) \tag{17}$$

where TP symbolizes either the viscosity η or the thermal conductivity λ, and TP^* accordingly symbolizes the associated factors H or L as given by Eqs. (5) and (10). The constant 1 was added to the transport property ratio to avoid a divergence of the logarithm at small viscosities and thermal conductivities in the gas region. With this transformation a substantial improvement of the transport equations of state was achieved over such formulations which used only the transport property ratio TP/TP^* as independent variable.

The functional form of the transport equation of state had evolved up to this point from an empirical search for suitable terms. The resulting structure resembled to a considerable extent the modified BWR equations of state. This similarity led to the idea to use a new optimization method, recently developed by Setzmann and Wagner,[62] in order to obtain more efficient transport equations of state in a systematic way. The equations which are presented in the sections below are the first results of this approach. As expected, the optimization procedure yielded different functional forms for the viscosity and the thermal conductivity but in both cases the number of adjustable parameters is smaller than in the earlier versions and the quality of the fit has been increased considerably. The "bank of terms" from which the most efficient functions were selected did not include exponential functions with powers higher than TP_R^2. Such terms have led to significant improvements of thermal equations of state and their use will no doubt result in further improved transport equations of state, too.

5.1. The Optimized Equation for the Viscosity

Due to its steep gradients at low temperatures a representation of the viscosity surface is more complicated than that of the thermal conductivity. For example, the values for oxygen in Table 4 vary by a factor of 48 between their extremes. These data were used as the base to determine the number of terms in the equation and the individual functional expressions. The potential of the optimization procedure may be appraised from the fact that the original equation[59,60] with 21 terms yielded a weighted sum of least squares of 75 whereas an optimized equation with the same number but different terms yielded a value of four. Reducing the number of terms to 15 resulted in an equation with a weighted sum of least squares of 30, still much less than the original equation. The equation finally accepted is

$$p_R = \sum_{i=1}^{13} f_i \, TP_R^{h_i} \, T_R^{t_i} + e^{-ITP_R^2} \sum_{i=14}^{20} f_i \, TP_R^{h_i} \, T_R^{t_i} \qquad (18)$$

with the exponents h_i and t_i, and the parameters f_i and I listed in Table 6. This equation is superior to the other variants because it reproduces the critical region particularly well. The quality of the representation is documented in Fig. 29 which shows percentage deviations between viscosities from Eq. (18) and the tabulated data for eighteen isotherms. The "breakdown" of the deviations at 70 K and 100 K suggests that the equation should not be extrapolated beyond 100 MPa at low temperatures. The same is indicated by the upward trend of the deviations above 800 K. The deviations at subcritical temperatures are well within ±3% including the representation of the saturation boundary. The near-critical 160 K isotherm is reproduced excellently. A maximum of the deviations occurs systematically from 200 K up at those pressures where the isotherms have an inflection point. The deviations exceed 3% in these cases between 200 K and 300 K. Already at 400 K the maximum is reduced to a deviation of 1.5%. The best representation is achieved between 500 K and 800 K with deviations smaller than ±0.5%.

This overview and the comparisons with the selected data sets confirm that the transport equation of state, Eq. (18), represents the viscosity of oxygen well within the uncertainties of the experimental data and may be used as an alternative to the residual correlation, Eqs. (2) and (4), with comparable accuracy.

5.2. The Optimized Equation for the Thermal Conductivity

Thermal conductivity surfaces have generally more moderate proportions and are easier to describe by correlating functions. The data for oxygen as given in Table 5 vary by a factor of twenty between the smallest and the highest value. Consequently, Setzmann and Wagner's optimization procedure yielded "shorter" functional forms than the original equation[59,60] throughout. The most compact equation required as little as ten terms but yielded a weighted sum of least squares still considerably smaller than the empirically structured formulation with 21 terms. The best representation of the thermal conductivity surface was obtained with the equation

$$p_R = \sum_{i=1}^{9} g_i \, TP_R^{l_i} + e^{-ITP_R^2} \sum_{i=10}^{17} g_i \, TP_R^{l_i} \, T_R^{t_i} \qquad (19)$$

which consists of nine polynomial terms in the linear part and eight terms associated with the exponential function. The exponents l_i, t_i and the parameters g_i and I are listed in Table 7. Fig. 30 shows percentage deviations between thermal conductivities from Eq. (19) and the tabulated data for eighteen isotherms. The quality of the representation can be rated excellent in the entire range. As for the viscosity equation of state, the downward trend of the deviations at 70 K and 100 K indicates a limited capability for extrapolations beyond 100 MPa. Aside from that, Eq. (19) can be used safely for extrapolations beyond the pressure and temperature limits of the tabulated data set. Negative deviations occur on the near-critical 150 K isotherm developing into an S-shape at 200 K but not exceeding a margin of −3%. The same deviation pattern is observed for the viscosity equation of state around the inflection points of the isotherms. For the thermal conductivity equation, however, the deviations remain within ±2% already at 240 K and reduce steadily to higher temperatures. The dilute gas thermal conductivity at 0.1 MPa is reproduced slightly too high at all temperatures (at the most 1.5% at 240 K). This deviation would not occur if the data by Geier and Schäfer had been used exclusively (cf. Fig. 12). This example underlines that the thermal conductivity equation

of state may be used to assess the reliability of experimental data. In a similar way, the experiences during the evolution of the equation led to an improved estimate of the "background" thermal conductivity at the critical point of oxygen.

The transport equation of state, Eq. (19), provides a representation of the thermal conductivity surface of oxygen equivalent to Eqs. (8) and (9) and can be used alternatively outside of the region where the critical enhancement becomes significant; see Fig. 28.

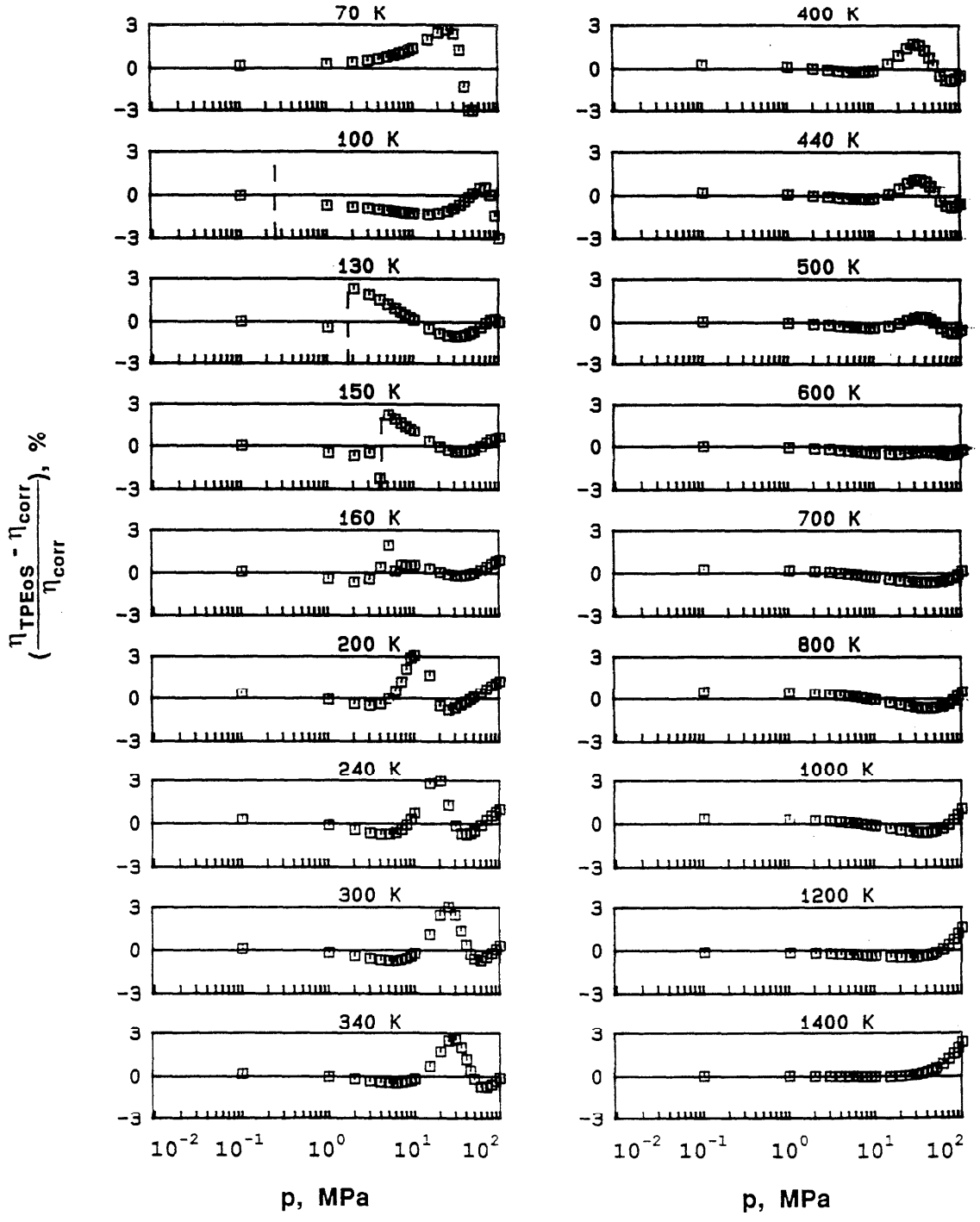

FIG. 29. Comparison of the transport equation of state (18) with the residual correlation for the viscosity of oxygen.

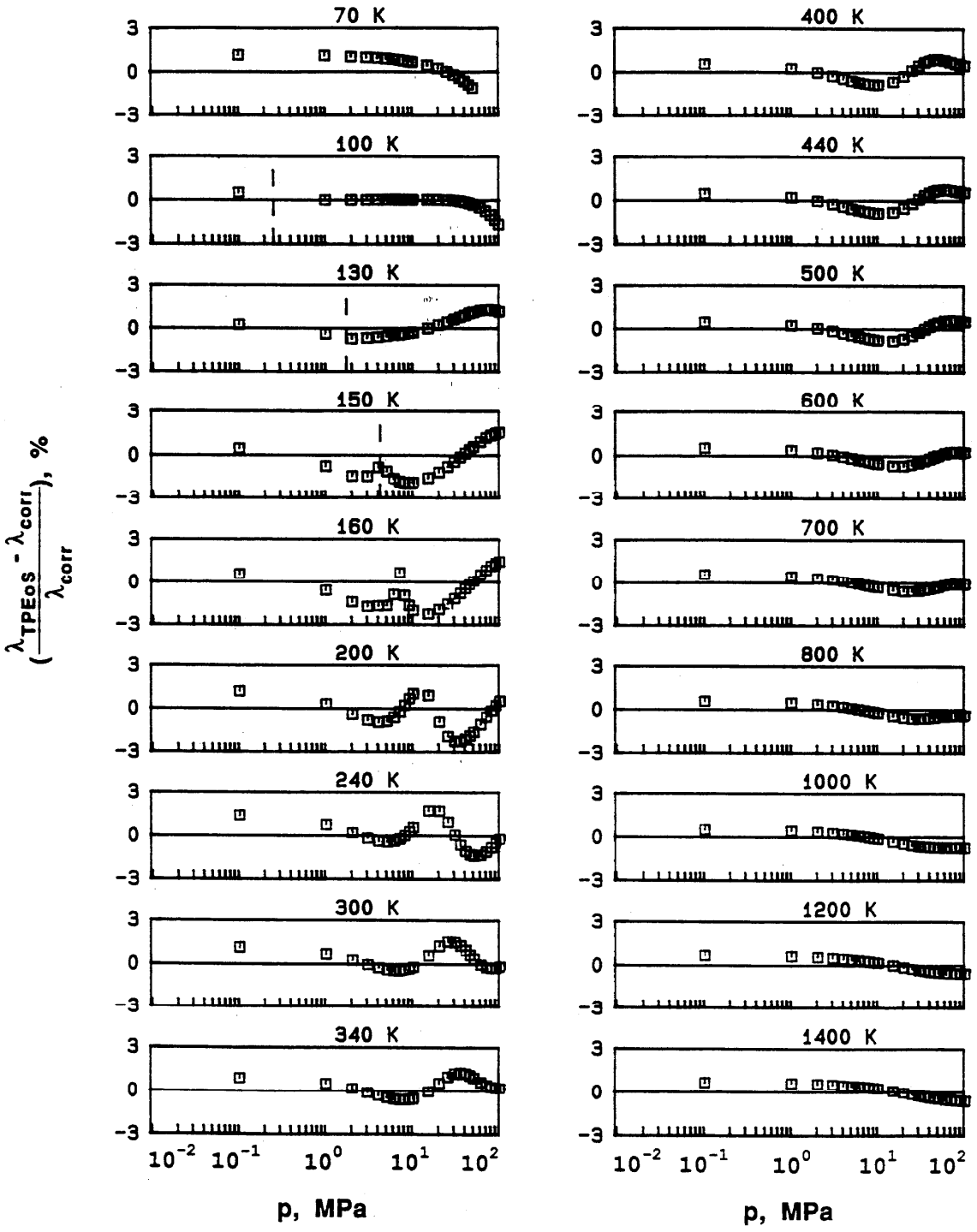

FIG. 30. Comparison of the transport equation of state (19) with the residual correlation for the thermal conductivity of oxygen.

TABLE 6. Numerical values of the exponents h_i, t_i, and parameters f_i of the transport equation of state for the viscosity of oxygen, eq. (18)

i	h_i	t_i	f_i
1	1	3.5	$-0.888\,521\,474\,5\cdot10^{-1}$
2	1	1	$-0.294\,691\,116\,3\cdot10^{2}$
3	1	0.5	$0.849\,113\,247\,7\cdot10^{2}$
4	1	0	$-0.561\,052\,183\,1\cdot10^{2}$
5	1	−2	4.216 610 109
6	1	−3.5	−0.459 748 184 7
7	3	2.5	0.491 444 826 7
8	3	0	−4.145 433 692
9	5	1	1.795 492 508
10	8	2	−0.171 481 750 7
11	9	2.5	$0.205\,222\,536\,3\cdot10^{-1}$
12	9	2	$0.287\,365\,721\,5\cdot10^{-1}$
13	10	2	$-0.253\,652\,801\,0\cdot10^{-2}$
14	1	3	$-0.775\,324\,913\,3\cdot10^{3}$
15	2	2	$0.174\,041\,703\,4\cdot10^{4}$
16	6	−2	$-0.349\,694\,130\,7\cdot10^{4}$
17	8	4	$-0.165\,463\,934\,6\cdot10^{5}$
18	11	3	$0.189\,932\,178\,1\cdot10^{6}$
19	12	9	$-0.140\,483\,330\,5\cdot10^{3}$
20	12	3	$-0.212\,010\,314\,1\cdot10^{6}$

$I = 15$

TABLE 7. Numerical values of the exponents l_i, t_i, and parameters g_i of the transport equation of state for the thermal conductivity of oxygen, Eq. (19).

i	l_i	t_i	g_i
1	1	1.5	$-0.347\,207\,079\,5\cdot10^{2}$
2	2	1	$0.355\,626\,395\,6\cdot10^{2}$
3	3	−3.5	$0.277\,303\,004\,3\cdot10^{-1}$
4	4	0.5	$-0.123\,323\,480\,7\cdot10^{2}$
5	5	0.5	2.644 052 895
6	7	−1	$-0.439\,610\,442\,4\cdot10^{-1}$
7	8	0	−0.109 296 592 0
8	8	−1	$0.102\,804\,225\,3\cdot10^{-1}$
9	10	2.5	$0.517\,459\,401\,1\cdot10^{-5}$
10	1	−2	7.780 108 761
11	2	2	−0.733 149 586 6
12	4	0	−4.110 880 170
13	5	0	3.987 963 895
14	10	0	$0.128\,183\,695\,0\cdot10^{-1}$
15	12	6	$-0.735\,967\,154\,2\cdot10^{10}$
16	14	1	$-0.101\,427\,980\,4\cdot10^{-4}$
17	15	1	$0.233\,944\,142\,9\cdot10^{-4}$

$I = 0.05$

6. Tolerances of the Evaluated Data and Recommendations for Additional Measurements

The experimental results which are available for the transport properties of oxygen are partially of quite differing quality. Even when narrowed down to those data which have been selected to generate the present tables, an estimation of their tolerances arrives at considerably higher margins than the tolerances assigned to the IUPAC thermodynamic tables. The estimated tolerances for the viscosity and thermal conductivity of oxygen are summarized in Fig. 31.

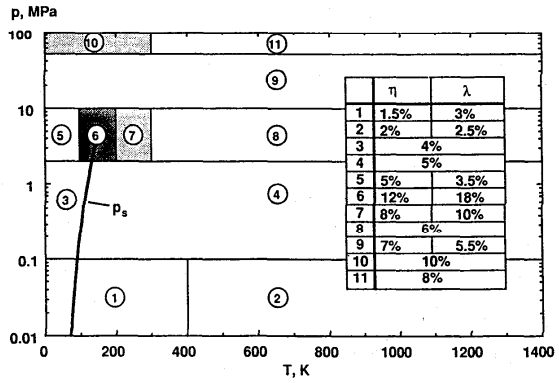

FIG. 31. Tolerances assigned to the evaluated data sets for the viscosity and thermal conductivity of oxygen (p_S — vapor pressure curve).

The range for which the transport properties of oxygen have been tabulated here represents a considerable extension compared to the region where measurements have been conducted. Neither the viscosity nor the thermal conductivity was measured at high pressures above 310 K. Such measurements would be valuable for the viscosity in order to complement the data of Haynes. Preferably, an oscillating disk instrument or a capillary viscometer should be used in such a study. There is also a need for measurements from 80 K down to the triple point. They should be conducted on isotherms to resolve the temperature dependence of the viscosity precisely.

In the case of the thermal conductivity the transient hot-wire data of Roder should be supplemented by data from other methods at high pressures above 310 K. No experimental data exist below 73 K. The contradictory data situation in the low-density region between 500 K and 1500 K should be settled by new measurements. Eventually, the temperature range should be extended to 2000 K. It would be useful in particular to explore the critical enhancement by measurements in a parallel-plate apparatus or by interferometry in order to resolve the discrepancies between the data of Roder and Weber. Unfortunately, there is not a great chance for such time-consuming studies since experimentalists seem to be enticed worldwide by the fast operation of the transient hot-wire technique. We hope that this attraction will not lead to the complete extinction of other thermal conductivity instruments.

7. Computer Programs

The correlations presented in this paper along with the necessary IUPAC formulation for the thermodynamic properties have been coded in FORTRAN. Initially, the evaluation of all thermophysical properties for one state point required 18 seconds execution time on a personal computer (68000 microprocessor, 8 MHz). This could be reduced to 1.5 seconds by reprogramming the fundamental equation of state and its derivatives. The properties which are relevant for heat and mass transfer calculations such as kinematic viscosity, thermal diffusivity, or the Prandtl number can be readily obtained by combining the basic routines. Requests for the code may be sent via electronic mail to ALSO@NISTCS2.BITNet.

8. Acknowledgments

Financial support for this research from Deutsche Forschungsgemeinschaft is gratefully acknowledged.

The project has been carried out on assignment of the Subcommittee on Transport Properties of the Commission I.2 of the International Union for Pure and Applied Chemistry. Valuable advice has been received from Professor J. Kestin, Chairman of the Subcommittee.

A. Laesecke wishes to acknowledge a postdoctoral fellowship awarded by the Royal Norwegian Council for Scientific and Industrial Research (NTNF) and a research stipend awarded by Deutsche Forschungsgemeinschaft. The hospitality of the staff and the excellent working conditions at the Thermophysics Division of NIST, Boulder, contributed substantially to the completion of this paper.

Finally, the authors thank Mrs. P. Leyens for her help in the computations toward the optimized transport equations of state.

9. References

[1]G. Baylie, Mechanical Engineering, Sept., 27 (1985).
[2]W. Wagner and K. M. de Reuck, International Thermodynamic Tables of the Fluid State. 9: Oxygen, Blackwell Scientific Publications, Oxford (1987).
[3]J. Kestin, The Transport Properties of Water Substance. Water and Steam, J. Straub and K. Scheffler, Eds., Pergamon Press, Oxford (1980).
[4]H. Preston-Thomas, Metrologia, **12**, 7 (1976).
[5]A. A. Clifford, P. Gray and A. C. Scott, J. Chem. Soc. Faraday Trans. I **71**, 875 (1975).
[6]G. P. Matthews, C. M. S. R. Thomas, A. N. Duffy, and E. B. Smith, J. Chem. Soc. Faraday Trans. I **72**, 238 (1976).
[7]A. V. Lavushchev and V. E. Lyusternik , Russ. J. Phys. Chem. **50**, 1795 (1976).
[8]J. Kestin and W. Leidenfrost, Physica **25**, 1033 (1959).
[9]I. F. Golubev, The Viscosity of Gases and Gas Mixtures, Israel Progr. Scientific Transl., Jerusalem, (1970).
[10]R. Kiyama and T. Makita , Rev. Phys. Chem. Japan **26**, 70 (1956).
[11]T. Makita, Mem. Fac. Ind. Arts, Kyoto Techn. University **4**, 19 (1955)
[12]W. M. Haynes, Physica **89A**, 569 (1977).
[13]H. J. M. Hanley, R. D. McCarty, and J. V. Sengers, Viscosity and Thermal Conductivity Coefficients of Gaseous and Liquid Oxygen, NASA CR Nr. 2440 (1974).
[14]B. A. Younglove, Thermophysical Properties of Fluids. I. Argon, ethylene, parahydrogen, nitrogen, nitrogen trifluoride, and oxygen. J. Phys. Chem. Ref. Data, **11** (1982), Supplement 1.
[15]H. J. M. Hanley and J. F. Ely, J. Phys. Chem. Ref. Data **2**, 735 (1973).
[16]J. Hellemans, J. Kestin, and S. T. Ro, Physica **65**, 362 (1973).
[17]C. J. G. Raw and C. P. Ellis, J. Chem. Phys. **28**, 1198 (1958).
[18]N. B. Vargaftik, Tables on the Thermophysical Properties of Liquids and Gases. 2nd Ed., Hemisphere Publ. Corp., Washington D. C. (1975).
[19]K. Stephan and K. Lucas, The Viscosity of Dense Fluids, Plenum Press, New York (1979).
[20]Japanese Society of Mechanical Engineers (JSME) Data Book, Thermophysical Properties of Fluids, (1983).
[21]G. C. Maitland and E. B. Smith, J. Chem. Eng. Data **17**, 150 (1972).
[22]W. A. Cole and W. A. Wakeham , J. Phys. Chem. Ref. Data **14**, 209 (1985).
[23]A. Bousheri, J. Bzowski, J, Kestin and E. A. Mason, J. Phys. Chem. Ref. Data **16** 445 (1987).
[24]N. S. Rudenko and L. N. Shubnikov, Phys. Z. Sowjetunion **6**, 470 (1934).
[25]H. Kamerlingh Onnes, Verh. Koningl. Akad. Wetenshapen, **21**, 1 (1881).
[26]N. S. Rudenko, Zh. Eksp. Teor. Fiz. **9**, 1078 (1939).
[27]Y. Saji and T. Okuda, Int. Adv. Cryogen. Engineering **10**. 209 (1964).
[28]W. Grevendonk, W. Herremann, W. de Presseroey and A. de Bock, Physica **40**, 207 (1968).
[29]J. Hellemans, H. Zink, and O. van Paemel, Physica **47**, 45 (1970).
[30]A. van Itterbeek, J. Hellemans, H. Zink, and M. van Cauteren, Physica **32**, 2171 (1966).
[31]A. de Bock, W. Grevendonk and H. Awouters, Physica **34** , 49 (1967).
[32]H. J. M. Hanley, R. D. McCarty, and W. M. Haynes, J. Phys. Chem. Ref. Data **3**, 979 (1974).
[33]H. M. Roder, Transport Properties of Oxygen, NAS*A* Ref. Publ. 1102, NBS Int. Rep. 82-1672 (1983).
[34]J. Stefan, Wiener Ber. **72**, 69 (1875).
[35]H. M. Roder, J. Res. Nat. Bur. Stds. **87**, 279 (1982).
[36]L. A. Weber, Int. J. Thermophys. **3**, 117 (1982).
[37]F. G. Keyes, Trans. ASME, **77**, 1395 (1955).
[38]H. Ziebland and J. *T.* A. Burton, Brit. J. Appl. Phys. **6**, 416 (1955).
[39]E. Borovik, Zh. Eksp. Teor. Fiz. **17**, 328 (1947).
[40]G. C. Maitland, M. Mustafa and W. A. Wakeham, J. Chem. Soc. Faraday Trans. **79**, 163 (1983).
[41]H. Geier and K. Schäfer. Allg. Wärmetechnik **10**. 70 (1961).
[42]S. C. Saxena and G. P. Gupta, Progr. Astronaut. Aeron. **23**, 45 (1970).
[43]P. C. Jain and S. C. Saxena, Mol. Phys. **33**, 133 (1977).
[44]H. L. Johnston and E. R. Grilly , J. Chem Phys. **14**, 233 (1946).
[45]N. V. Tsederberg, Teploenergetika **4**, 45 (1957).
[46]Z. A. Ivanova, N. V. Tsederberg, and V. N. Popov, Thermal Engng. **14**, 98 (1967).
[47]A. N. G. Pereira and C. J. G. Raw, Phys. Fluids **6**, 1091 (1963).
[48]A. A. Vassermann and V. A. Rabinovich, Thermophysical Properties of Liquid Air and its Components, Israel Progr. Scientific Transl., Jerusalem (1970).
[49]E. U. Franck, Z. Elektrochem. **55**, 636 (1951).
[50]A. A. Westenberg and N. de Haas, Phys. Fluids **6**, 617 (1963).
[51]Y. S. Touloukian, P. E. Liley, and S. C. Saxena, Thermophysical Properties of Matter. Vol. 3: Thermal Conductivity of Nonmetallic Liquids and Gases. Plenum Press, New York, 1970.
[52]N. B. Vargaftik, L. P. Filippov, A. A. Tarzimanov, and E. E. Tozkij, The Thermal Conductivity of Liquids and Gases, Izd. Standartov, Moscow (1978) (in Russian).

[53]R. C. Reid, J. M. Prausnitz, and B. E. Poling, The Properties of Gases and Liquids, 4th ed., McGraw-Hill, New York (1987).
[54]R. D. McCarty, Interactive FORTRAN Programs for Micro Computers to Calculate the Thermophysical Properties of Twelve Fluids (MIPROPS), NBS Tech. Note. 1097 (1986).
[55]G. J. Sherman, J. W. Magee, and J. F. Ely, Int. J. Thermophysics **10**, 47 (1989).
[56]G. A. Olchowy and J. V. Sengers, Phys. Rev Lett. **61**, 15 (1988).
[57]G. A. Olchowy and J. V. Sengers, Int. J. Thermophys. **10**, 417 (1989).
[58]A. Laesecke and K. Stephan, Representation of the Viscosity of Water in Terms of Pressure and Temperature. In: Proc. 10th Int. Conf. Prop. Steam, MIR Publishers, Moscow, **1**, 399 (1986).
[59]A. Laesecke, Viskosität und Wärmeleitfähigkeit als thermodynamische Zustandsgrössen und ihre Darstellung durch Zustandsgleichungen, Fortschr.-Ber. VDI, Reihe 3, Nr. 117, VDI-Verlag, Düsseldorf (1986).
[60]K. Stephan, R. Krauss, and A. Laesecke, J. Phys. Chem. Ref. Data **16**, 993 (1987).
[61]R. Krauss, unpublished results.
[62]U. Setzmann and W. Wagner, Int. J. Themophys. **10**, 1103 (1989).